Review Article

ADVANCED PHOTONICS

Roadmap for single-molecule surface-enhanced Raman spectroscopy

Yang Yu,[a,†] Ting-Hui Xiao,[b,†,*] Yunzhao Wu,[b] Wanjun Li,[a] Qing-Guang Zeng,[a] Li Long,[c] and Zhi-Yuan Li[c,*]
[a]Wuyi University, School of Applied Physics and Materials, Jiangmen, China
[b]University of Tokyo, Department of Chemistry, Tokyo, Japan
[c]South China University of Technology, School of Physics and Optoelectronics, Guangzhou, China

Abstract. In the near future, single-molecule surface-enhanced Raman spectroscopy (SERS) is expected to expand the family of popular analytical tools for single-molecule characterization. We provide a roadmap for achieving single molecule SERS through different enhancement strategies for diverse applications. We introduce some characteristic features related to single-molecule SERS, such as Raman enhancement factor, intensity fluctuation, and data analysis. We then review recent strategies for enhancing the Raman signal intensities of single molecules, including electromagnetic enhancement, chemical enhancement, and resonance enhancement strategies. To demonstrate the utility of single-molecule SERS in practical applications, we present several examples of its use in various fields, including catalysis, imaging, and nanoelectronics. Finally, we specify current challenges in the development of single-molecule SERS and propose corresponding solutions.

Keywords: surface-enhanced Raman spectroscopy; plasmonics; single-molecule SERS.

Received Dec. 9, 2019; accepted for publication Feb. 3, 2020; published online Feb. 26, 2020.

© The Authors. Published by SPIE and CLP under a Creative Commons Attribution 4.0 Unported License. Distribution or reproduction of this work in whole or in part requires full attribution of the original publication, including its DOI.

[DOI: 10.1117/1.AP.2.1.014002]

1 Introduction

Raman spectroscopy is a powerful analytical tool that probes vibrational fingerprints of molecules and enables high-content analysis of composite systems of physical, chemical, and biological interests by virtue of its inherent specificity. As an optical technique, Raman spectroscopy is noninvasive and versatile for studying solid, liquid, and gas samples and has been used for various applications, such as chemical detection, disease diagnosis, and environmental monitoring.[1] However, Raman spectroscopy suffers from low sensitivity, as spontaneous Raman scattering is intrinsically very weak. Only about 1 in $\sim 10^7$ photons that interact with molecules undergoes Raman scattering.[2] The low sensitivity of Raman spectroscopy severely limits its practical applications, which range from trace-amount molecular detection to real-time bioimaging.

Surface-enhanced Raman spectroscopy (SERS), as a surface-sensitive Raman technique that enables significant enhancement of Raman signals of adsorbed molecules on an engineered surface, has been considered as a promising technique to overcome the low sensitivity of traditional Raman spectroscopy.[3,4] Compared with the traditional Raman spectroscopy that is based on spontaneous Raman scattering, SERS with state-of-the-art performance is capable of offering extremely high sensitivity, up to single-molecule detection level.[5] Even though the exact enhancement mechanism of SERS is still in debate, especially for those cases with extremely high enhancement factors, it is generally accepted that two underlying mechanisms, namely electromagnetic mechanism (EM)[6,7] and chemical mechanism (CM),[8,9] dominate in the Raman enhancement.

The EM is a long-range effect that originates from an enhanced electromagnetic field and normally provides a much higher enhancement than the CM.[10] The enhanced electromagnetic field increases the number of photons interacting with molecules and thus increases the number of photons undergoing Raman scattering. Traditionally, the electromagnetic field enhancement is achieved through the excitation of surface plasmon resonance (SPR) on roughened or periodically structured metal substrates.[11,12] This is because the collective oscillation of free electrons enabled by the SPR is capable of localizing and concentrating incident light on the surface of the metal substrates. Conventionally, it is not challenging to achieve

*Address all correspondence to Ting-Hui Xiao, E-mail: xiaoth@chem.s.u-tokyo.ac.jp; Zhi-Yuan Li, E-mail: phzyli@scut.edu.cn

†These authors contributed equally to this work.

a SERS enhancement factor above $\sim 10^7$ for metal substrates with SPR.[13] On the other hand, dielectric nanostructures with strong structural resonance, such as silicon and germanium nanodisks with Mie resonance,[14,15] have also been implemented for SERS by virtue of localized electromagnetic field enhancement.[16,17] A SERS enhancement factor of up to $\sim 10^3$ has been experimentally demonstrated by utilizing EM.[18] Even though such an enhancement factor is moderate and hardly comparable with those of SPR-based metal substrates, dielectric substrates have several other advantages, such as low photothermal heat generation and excellent biocompatibility, and thus they have emerged as promising alternatives for SERS applications.

The CM is a short-range effect related to the charge transfer between surface-adsorbed molecules and the substrate.[19] The charge transfer resonance increases the Raman polarizability of the molecules, thereby leading to increased Raman-scattering cross-sections. In addition to noble metals, two-dimensional (2-D) materials including graphene, MoS_2, and h-BN as well as semiconducting metal oxides including TiO_2, CuO, and Ta_2O_5 have been explored for SERS applications by virtue of charge transfer resonance.[6,20–24] A state-of-the-art chemical enhancement factor up to $\sim 10^7$ has been demonstrated recently.[25] Although such an enhancement factor achieved by the CM is still much smaller than that of the EM counterpart (above $\sim 10^{10}$),[26] the CM offers a parallel path to enhance Raman signals, which enables synergic Raman enhancement by combination of EM and CM and relaxes the extreme requirement of electromagnetic-field enhancement for single-molecule SERS.

Single-molecule SERS, as the ultimate goal of SERS in sensitivity, has attracted great interest since it was first reported around 20 years ago.[27,28] The emergence of single-molecule SERS has not only stimulated rapid development of nanotechnology but also provided an unprecedentedly high-content and ultrasensitive optical method for chemical analysis. By virtue of the recent development of nanotechnology, single-molecule SERS is becoming accessible to more and more researchers in the SERS field. It has already become a promising tool to study chemical catalysis, cell biology, and nanoelectronics.[29–36] A variety of strategies for realizing single-molecule SERS have been proposed while a number of novel applications based on single-molecule SERS have been demonstrated. However, single-molecule SERS is still facing some critical challenges that limit its practical utility. In this review, we systematically discuss the recent development of single-molecule SERS, starting from a conceptual introduction and ending at an analysis of current challenges. We hope this review can provide a relatively complete picture of the current research status of single-molecule SERS and arouse more interest and inspiration to further promote the development of this research field. The review is organized as follows. In Sec. 2, we give a brief introduction of single-molecule SERS, which clarifies several crucial conceptual points for study of single-molecule SERS. In Sec. 3, we summarize and categorize the strategies for realizing single-molecule SERS, including electromagnetic enhancement, chemical enhancement, resonance enhancement, and other potential strategies. In Sec. 4, we review several important applications enabled by single-molecule SERS. In Sec. 5, we discuss current challenges for single-molecule SERS and propose the corresponding perspectives. In Sec. 6, we give a summary of this review.

2 Single-Molecule SERS

Single-molecule SERS is not just an ultrasensitive version of traditional SERS. In terms of science, single-molecule SERS opens up a new window to observe subtle spectroscopic phenomena in single molecules without statistical average. For example, the true homogeneous and inhomogeneous broadening of Raman peaks was observed and experimentally verified using single-molecule SERS.[37,38] In terms of applications, single-molecule SERS significantly expands the application region of Raman spectroscopy. By employing single-molecule SERS, real-time monitoring of reduction–oxidation reaction and catalytic reaction at the single-molecule level was technically realizable,[29–31] which can be used to guide design of heterogeneous biocatalysts with supreme catalytic activity. Compared with some other techniques, such as super-resolution fluorescence microscopy, single-molecule SERS possesses both pros and cons. In terms of spatial resolution, the state-of-the-art single-molecule SERS (TERS) is capable of visualizing single molecules with a subnanometer resolution,[39] which outperforms typical super-resolution fluorescence microscopy with a spatial resolution of tens of nanometers. In addition, single-molecule SERS probes the vibrational modes of single molecules, thus providing high-content structural information of molecules and circumventing the requirement for labeling, which is essential for super-resolution fluorescence microscopy. However, single-molecule SERS imaging is hardly applicable for large-area imaging due to the tiny size and sparse distribution of hotspots. In terms of temporal resolution, the state-of-the-art single-molecule SERS enables a high frame rate up to 800,000 frames/s,[40] which is superior to the state-of-the-art super-resolution fluorescence microscopy that is able to achieve a high frame rate of 100 frames/s.[41] Single-molecule SERS has already demonstrated its promising potential and is expected to find diverse applications in future. However, several crucial points need to be addressed for implementation of single-molecule SERS as several new challenges appear when the concentration of detected molecules is decreased down to the single-molecule level.

2.1 Enhancement Factor of Single-Molecule SERS

The required enhancement factor for single-molecule SERS is a basic and critical value that can help researchers intuitively estimate how difficult it is to realize SERS detection with single-molecule sensitivity. Unfortunately, this value is still controversial. When the single-molecule SERS was first observed around 20 years ago, it was claimed that an enhancement factor of $\sim 10^{14}$ was essential for single-molecule detection.[27,28] However, the EM-induced enhancement factor by the SERS substrates was only $\sim 10^{10}$,[26] which can hardly be used to account for the high enhancement factor for single-molecule detection. A number of efforts have been made to explain this large enhancement gap by considering new enhancement mechanisms, such as chemical enhancement and resonance Raman enhancement.[42] Later on, it was argued that an enhancement factor of $\sim 10^8$ is sufficient for realizing single-molecule detection.[43] It is worthwhile to note that the sensitivity of SERS measurement does not only rely on SERS substrates but also relies on the detected molecules and the optical setup used for the measurement. On the one hand, various molecules may exhibit various Raman polarizabilities under the same SERS measurement condition. Especially, when the photon

energy of excitation light accidentally satisfies the electronic transition of a specific molecule, resonance Raman scattering occurs, which is capable of providing an enhancement of Raman polarizability up to $\sim 10^6$.[44] The difference in the Raman polarizability results in the difference of the lowest detectable concentrations for different molecules. On the other hand, even for the same type of molecules, the sensitivities or detection limits of SERS measurement may also be different using different optical setups.[45] The parameters of optical components in the optical setups, such as numerical apertures of objective lens, sensitivities of spectrometers, wavelengths of incident light, and polarization states of incident light, also significantly influence the sensitivity of SERS measurement.[46] The numerical apertures determine the collection efficiency of Raman scattering for the SERS measurement. A high numerical aperture enables a high collection efficiency, which is beneficial for improving the sensitivity for SERS measurement.[47] The sensitivity of the spectrometer used for the SERS measurement determines the lowest Raman intensity coupled to the spectrometer that can be detected. A high sensitivity of the spectrometer enables a low detectable Raman intensity, which is also desired for increasing the sensitivity of SERS measurement. Moreover, the excitation wavelength and polarization state of the incident light determine the excitation of SPR on the SERS substrate. When the excitation wavelength is selected at the resonance wavelength of SPR while the polarization state is selected for the highest electromagnetic enhancement of the SERS substrate, the enhanced Raman signal is the strongest.[48] This indicates that the selection of an optimum excitation wavelength and an optimum polarization state of the incident light can also be utilized for increasing the sensitivity of the SERS measurement. In summary, the required single-molecule SERS enhancement factor varies for different molecules at different experimental conditions.

How to experimentally estimate the enhancement factor of single-molecule SERS is another important point that needs to be taken care of (see Refs. 26–29). The enhancement factor of single-molecule SERS is defined identically to that of conventional SERS, which can be obtained by comparing Raman intensities of the same type of molecules with and without enhancement of SERS substrates. For the measurement without enhancement of SERS substrates, which is the ground truth for estimation of the enhancement factor, the concentration of the measured sample is relatively high. Molecular solutions are preferred as the samples for the ground truth measurement as their molecular concentrations are precisely controllable. For the measurement with enhancement of SERS substrates, the concentration of the measured sample is extremely low. Especially for single-molecule detection, the concentration of the measured sample needs to be decreased to the level at which only one molecule on average exists in a measured volume. Such low concentration is probable to result in an inhomogeneous distribution of molecules adsorbed on the SERS substrates. Therefore, the practical concentration of molecules in the measured volume on the SERS substrate requires prudential calibration. Some experimental evidences are conventionally needed to verify the practical concentration is at the single-molecule level.

2.2 Experimental Evidences of Single-Molecule SERS

SERS intensity fluctuation is one of the representative experimental evidences of single-molecule SERS. The fluctuation is partially due to the instability of surfaces of SERS substrates. The migration of surface atoms of SERS substrates (e.g., amorphous Au substrates) can influence the measured single-molecule signal.[40] Moreover, when the concentration of molecules is at the single-molecule level, only one molecule on average exists in the measured volume. The average here indicates the average in both time and space domains. As the current single-molecule SERS is mainly achieved by the SPR-based EM, hotspots with electromagnetic field enhancement high enough for single-molecule detection are sparsely distributed in the measured volume. Thus, there is a large probability that the single molecule that dynamically moves in the measured volume does not locate at the hotspots at any time. This means that if we continuously monitor the SERS intensity of the single-molecule sample in time and space domains, the SERS intensity is expected to strongly fluctuate due to the dynamic motion of the single molecule in and out of the hotspots.[49–53]

Bianalyte approach is capable of offering more experimental evidence of single-molecule SERS. In this approach, a mixture of two analytes with distinguishable Raman spectra is used as the sample for the SERS measurement.[54,55] When the sample concentration is high, more than one molecule locates at the hotspots within the measured volume. The measured SERS signal is expected to be a mixture of the SERS spectra of both analytes. If the sample concentration is gradually decreased, and finally to the single-molecule level, only one molecule on average exists within the measured volume. The measured SERS signal is expected to come from only one of the two analytes. If we continuously monitor the SERS spectrum of the bianalyte sample in time and space domains at such concentration, the measured SERS spectrum is the spectrum of either one analyte or the other, rather than the mixture of two spectra. This phenomenon observed using the bianalyte approach can be used as another experimental evidence of single-molecule SERS.

2.3 Data Analysis of Single-Molecule SERS

As we have discussed in the last part, the SERS signals will fluctuate in time and space domains when the concentration of detected molecules is decreased down to the single-molecule level. It is essential to employ statistical methods to analyze the experimental data of single-molecule SERS. In order to make full use of statistical soundness, a sufficient number of SERS spectra need to be measured for statistical analysis. Principal component analysis (PCA) as a classical analytical method is widely used for characterization of single-molecule SERS.[56–58] For example, the PCA is powerful for decomposition of SERS spectra of a mixture in the bianalyte approach. The decomposition with statistical soundness is usable for characterization of SERS substrates, such as precise estimation of resonance wavelengths of hotspots and evaluation of enhancement efficiencies of SERS substrates. In addition, digitization of SERS intensities has been used for quantification of molecular concentration in single-molecule SERS. An intensity threshold is set to digitize single-molecule SERS signals with intensity fluctuation.[45,59] Based on the digitization, a calibration curve indicating the correlation between the signal intensity and sample concentration is constructed, which can be used for quantification of the sample at an extremely low concentration. Moreover, cluster analysis is also usable for classification of measured SERS spectra of a mixture in the bianalyte approach based on the correlation between the measured SERS spectra and the ground-truth spectra

of two target molecules. The cluster analysis method partitions the measured SERS spectra into two groups of similar spectra, which correspond to two target molecules.[56] Recently, the emergence of advanced chemometric techniques, such as least-square regression and artificial neural networks, provides the possibility for quantitative analysis of detected molecules by SERS measurement as it provides much deeper analysis of variables implied in the measured SERS spectra. Deep learning as a popular data analysis method is advantageous for classification of complex mixed analytes with a large number of features in the measured SERS spectra. Rapid classification of honey varieties has been recently demonstrated using deep learning to analyze the measured SERS spectra.[60] More data analysis methods with strong statistical soundness are desirable in the future to improve the reproducibility and quantification of single-molecule SERS.

3 Strategies for Single-Molecule SERS

In SERS theory, Raman enhancement factor enabled by EM is proportional to the fourth power of the local electric-field enhancement,[61] which is expressed as

$$G(r_0) = |E(r_0,\omega)|^4/|E_0(r_0,\omega)|^4, \tag{1}$$

where $E_0(r_0,\omega)$ is the electric field of the incident light while $E(r_0,\omega)$ is the localized electric field at the hotspot. The corresponding enhanced Raman intensity is expressed as

$$\begin{aligned} I(\omega_R) &= AG(r_0)|\alpha(\omega_R,\omega)|^2 I_0(r_0,\omega) \\ &= AI_0(r_0,\omega)|\alpha(\omega_R,\omega)|^2 \times |E(r_0,\omega)|^4/|E_0(r_0,\omega)|^4, \end{aligned} \tag{2}$$

where A is a coefficient related in practice with the collection efficiency of the optical system used to collect the Raman signal, $\alpha(\omega_R,\omega)$ is the Raman polarizability of the detected molecule, and $I_0(r_0,\omega)$ is the intensity of incident light. Based on Eq. (2), we know that there are two main strategies we can utilize for enhancing the sensitivity of SERS measurement using a specific optical system. One is to increase the local electric-field enhancement, which corresponds to the EM. The other is to increase the Raman polarizability of the detected molecule, which corresponds to the CM. In Sec. 3, we will introduce several EM-based and CM-based strategies for single-molecule SERS, which include electromagnetic enhancement, chemical enhancement, resonance enhancement, and other potential strategies.

3.1 Electromagnetic Enhancement

Electromagnetic enhancement, as the most widely used strategy for SERS, plays a fundamental role in single-molecule SERS. At the early stage of SERS development, metal substrates with rough surfaces were used, which were capable of offering decent Raman enhancement for detected molecules.[62–67] However, such metal substrates without delicate morphological designs can hardly satisfy the need for single-molecule detection due to their insufficient electromagnetic enhancement. Later on, extremely high electromagnetic enhancement has been demonstrated, which enables the measurement of SERS signals of nonresonant molecules with Raman differential cross sections typically in the range of 10^{-29} to 10^{-30} $\mathrm{cm}^2/\mathrm{sr}$. Blackie et al.[68] demonstrated single-molecule SERS of two nonresonant molecules, 1,2-di-(4-pyridyl)-ethylene (BPE) and adenine with enhancement factors of 5×10^9 and 10^{11}, respectively. The experiment not only verifies the capability of SERS for detecting nonresonant molecule at the single-molecule level but also provides quantitative enhancement factors required for single-molecule SERS detection of nonresonant molecules. However, single-molecule SERS with high reproducibility still remains a challenge. In this section, we will introduce several recently developed designs with highly controllable morphological structures that enable simultaneously high electromagnetic enhancement and reproducibility for single-molecule SERS.

3.1.1 Plasmonic nanogaps with precise size control

Plasmonic nanogaps, as a representative type of simple and effective structures for SERS applications, are frequently utilized for single-molecule SERS as they are capable of providing extremely high electromagnetic enhancement. However, the enhancement factors enabled by plasmonic nanogaps are highly sensitive to the sizes of nanogaps. Nanometer-scale error in the size can lead to an enhancement factor difference up to several orders of magnitude. Plasmonic nanogaps with precise size control are essential for single-molecule SERS as they are capable of offering controllable ultrahigh electromagnetic enhancement and excellent reproducibility. Several specific plasmonic nanogaps with controllable gap sizes will be introduced in this section.

In 2003, Wang et al.[47] for the first time demonstrated an optical antenna to observe the highly directional emission of Raman scattering from single molecules. The optical antenna consists of a silver ring and a silver dimer with a precise size control as shown in Fig. 1(a). By virtue of the strong electromagnetic enhancement of the plasmonic nanogap in the silver dimer, the directional emission of Raman signals from single molecules can be observed in the far-field. The single-molecule SERS spectra of R6G-d0/R6G-d4 enabled by the optical antenna are shown in Fig. 1(b). A distinct difference is observed between the two spectra, which is useful for distinguishing isotopologues. More importantly, with the precise size control of the plasmonic nanogap, an unprecedented near-unity fraction of the optical antennas has single-molecule sensitivity, indicating their excellent reproducibility for single-molecule SERS. In 2010, Lim et al. proposed and experimentally demonstrated a gold-silver core-shell nanodumbbell (GSND) with an engineerable nanogap for highly reproducible single-molecule SERS.[69] The GSND consists of two gold-silver core-shell nanoparticles linked by a single DNA molecule as shown in Fig. 1(c). It is fabricated with a high-yield synthetic method using a single-target-DNA hybridization, which is achieved by interconnecting two DNA sequences. One of the two DNA sequences, which is linked to a gold nanoparticle, is used to precapture a target Raman-active molecule, and then hybridized with the other DNA sequence, which is linked to another gold nanoparticle. The hybridization process enables linking the two gold nanoparticles as well as locating the target molecule within the nanogap of the two gold nanoparticles. Silver shells with precisely controllable thickness are subsequently grown on the surfaces of the two gold nanoparticles to engineer the gap size. The single-molecule SERS signals measured by the fabricated GSND are shown in Fig. 1(d). Due to the precise size-controllability of the fabrication method, SERS detection with single-molecule sensitivity and high reproducibility was successfully achieved.[69]

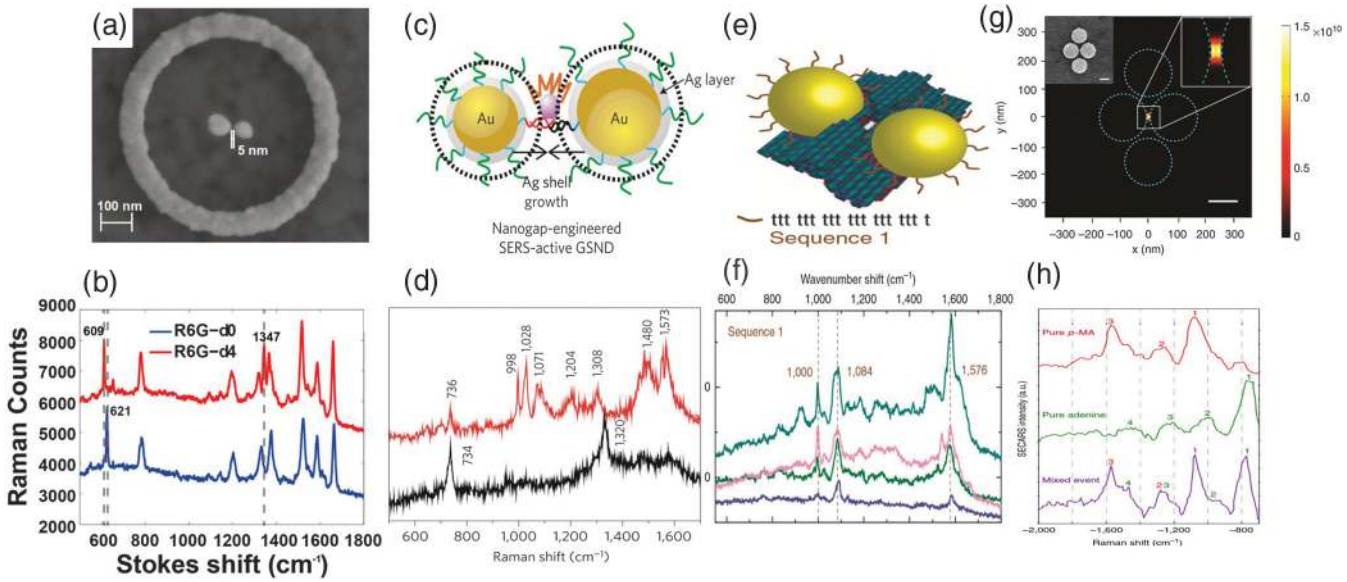

Fig. 1 Plasmonic nanogaps with precise size control for single-molecule SERS. (a) Scanning electron microscope image of an optical antenna. Inner and outer radii of silver rings are 300 and 380 nm, respectively. Left-hand rod is 80 nm long and 70 nm wide. Right-hand rod is 68 nm long and 62 nm wide. (b) Representative Raman spectra of R6G-d0 and R6G-d4 single-molecule level events. The R6G-d4 spectrum is shifted in the vertical direction by 2000 counts for display purposes.[47] (c) Nanometer-scale silver-shell growth-based gap-engineering in the formation of the SERS-active GSND. (d) Raman spectra taken from Cy3-modified oligonucleotides (redline) and Cy3-free oligonucleotides (blackline) in NaCl-aggregated silver colloids.[69] (e) Schematic of the NP dimers assembled on the DNA origami platform. The NPs are coated with an ssDNA brush to prevent aggregation as well as facilitate attachment to the origami platform. (f) Measured Raman spectra of the ssDNA coating of 19 bases of thymine (sequence 1) on the NP dimers.[70] (g) SECARS enhancement map. (h) Three representative SECARS spectra showing a pure *p*-MA event (top), a pure adenine event (middle), and a mixed event (bottom).[48] Figures reprinted with permission: (a) and (b) Ref. 47, © 2013 by the American Chemical Society; (c) and (d) Ref. 69, © 2009 by the Nature Publishing Group; (e) and (f) Ref. 70, © 2014 by the Nature Publishing Group; and (g) and (h) Ref. 48, © 2014 by the Nature Publishing Group.

Thacker et al.[70] proposed and experimentally realized a similar plasmonic nanogap with a controllable gap size based on a DNA origami technique. The proposed fabrication technique is advantageous for accurate positioning of nanoparticles. Gold nanoparticle dimers with reliable sub-5-nm nanogaps were successfully fabricated using the DNA origami technique, which is shown in Fig. 1(e). A high Raman enhancement factor of $\sim 10^7$ with high reproducibility was realized as shown in Fig. 1(f). The results clearly exhibit the promising potential of this building technique for highly reproducible single-molecule SERS.[70]

Coherent anti-Stokes Raman scattering (CARS) as a specific four-wave mixing process involves the coherent interaction of two pump waves, one Stokes wave, and one anti-Stokes wave through the third-order polarizability of the vibronic modes of a molecule.[48] The CARS signal is conventionally obtained by measuring the anti-Stokes wave generated with the input of two pump waves and one Stokes wave in the four-wave mixing process. By virtue of the molecular coherence, CARS signal is usually orders of magnitude stronger than spontaneous Raman signal. However, compared with SERS, conventional surface-enhanced CARS (SECARS) suffers from relatively low enhancement factors due to time-scale effects. Zhang et al.[48] proposed a plasmonic nanogap with Fano resonance for single-molecule SECARS with an enhancement factor up to 10^{11}. By combination of high electromagnetic enhancement of the nanogap and high sensitivity of nonlinear Raman spectroscopy, single-molecule sensitivity was experimentally realized. The plasmonic nanogap was formed by a plasmonic quadrumer, as shown in Fig. 1(g), which was fabricated by a standard complementary metal oxide semiconductor process. Electron-beam lithography was used to define its pattern and precisely control its size. With such a design, the plasmonic nanogap enables simultaneous electromagnetic enhancement of pump light, Stokes scattering, and anti-Stokes scattering. A total enhancement factor of $\sim 10^{11}$ over spontaneous Raman signal was experimentally realized for single-molecule detection. The bianalyte approach was also used to experimentally verify the capability of the proposed technique for single-molecule detection, as shown in Fig. 1(h). At the low concentration, either the SECARS spectrum of *p*-MA or adenine was measured for a mixed sample, exhibiting the signature of single-molecule detection.[48]

3.1.2 Plasmonic sharp tips

Plasmonic sharp tips are another type of configuration that enables ultrahigh Raman enhancement for single-molecule SERS.

This is mainly due to their sharp geometric configuration that is capable of realizing high concentration and localization of electromagnetic field. Besides chemically synthesized nanoparticles with sharp tips (e.g., sea-urchin-like nanoparticles),[71] another representative technique based on the plasmonic sharp tips is tip-enhanced Raman spectroscopy (TERS), which combines a plasmonic sharp tip with a controllable mechanical system with a shifting precision of subnanometer. TERS, as an extension technique of SERS, not only provides a single-molecule sensitivity but also enables Raman measurement in space domain with a subnanometer resolution.

In 2011, Liu et al.[72] used fishing-mode TERS to study the molecular structure of single-molecule junctions in different conduction states. The fishing-mode TERS, as shown in Fig. 2(a), is capable of simultaneously measuring conductance and TERS signals of a single-molecule junction locating at the apex of a sharp gold tip. A bias voltage is applied between the tip and a gold substrate to tune the conduction states of the single-molecule junction. The measured TERS signals of a 4,4'-bipyridine (4bipy) molecular junction around Raman peak of 1609 cm^{-1} at different voltages are shown in Fig. 2(b). By virtue of the high sensitivity of the plasmonic sharp tip, the

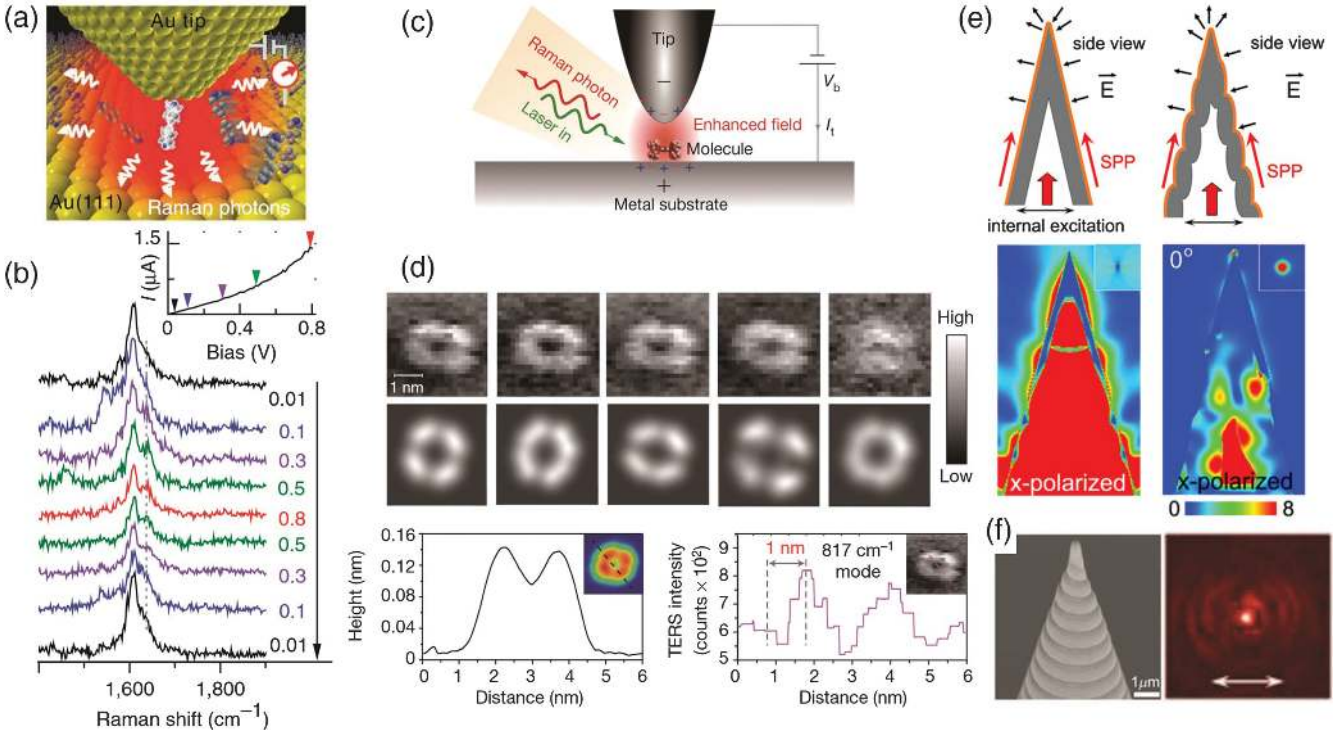

Fig. 2 Plasmonic sharp tips for single-molecule SERS. (a) An illustration of the FM-TERS system for simultaneous conductance and TERS measurement of single-molecule junctions. A gold (111) surface is preadsorbed with molecules. The distance between the gold tip and the gold (111) surface is then controlled by an STM equipped with a conductance-measuring circuit. The red contour indicates the distribution of electromagnetic field strength between the tip and the substrate. Wavy arrows indicate Raman scattering by the molecules. (b) The Raman band of 4bipy (1609 cm^{-1}) is seen to change with the bias voltage. Inset: current versus bias curve for 4bipy obtained with a mechanical break-junction setup.[72] (c) Schematic of tunneling-controlled TERS in a confocal-type side-illumination configuration, in which V_b is the sample bias and I_t is the tunneling current. (d) The top panels show experimental TERS mapping of a single molecule for different Raman peaks (23 × 23, ~0.16 nm per pixel), processed from all individual TERS spectra acquired at each pixel (120 mV, 1 nA, 0.3 s; image size: 3.6 × 3.6 nm^2). The middle panels show the theoretical simulation of the TERS mapping. The left bottom panel shows a height profile of a line trace in the inset STM topograph (1 V, 20 pA). The right bottom panel shows a TERS intensity profile of the same line trace for the inset Raman map associated with the 817 cm^{-1} Raman peak.[73] (e) The hollow conical taper and the taper with spiral corrugations along the conical surface (top panel). The simulated *E*-field intensity distributions in the *x*-*z* plane for the two structures with *x*-polarized incident light at the wavelength of 800 nm (bottom panel). (f) The side-view SEM image of fabricated spiral taper (left panel) and the false-color image of focus pattern of gold-coated spiral taper under linearly polarized excitation with *x*-direction polarization (right panel).[74] Figures reprinted with permission: (a) and (b) Ref. 72, © 2011 by the Nature Publishing Group; (c) and (d) Ref. 73, © 2013 by the Nature Publishing Group; and (e) and (f) Ref. 74, © 2014 by Wiley-VCH Verlag.

splitting of the Raman peak of the single-molecule junction was observed at a high bias voltage, which is inaccessible by other methods. Zhang et al.[73] utilized TERS for chemical mapping of a single molecule as shown in Fig. 2(c). By a combination of high electromagnetic enhancement of a plasmonic sharp tip and precise tuning capability of a scanning tunneling microscopy (STM), TERS mapping of a single molecule with a subnanometer spatial resolution for different vibrational modes was realized, which is shown in Fig. 2(d).[73] The above results verify that plasmonic sharp tips are an ideal and promising geometric configuration for single-molecule SERS.

However, experimental fabrication of these plasmonic sharp tips with extremely sharp apexes composed of several metal atoms to satisfy the requirement of ultrahigh electromagnetic enhancement for single-molecule SERS remains a challenge. As we have discussed in Sec. 2.1, the SERS sensitivity for a specific molecule does not only depend on the enhancement factors of SERS substrates but also on other experimental conditions. The conventional plasmonic sharp tips in TERS suffer from low transfer efficiencies of input light from light sources to hotspots of the sharp tips, which results in extremely high requirement of electric-field enhancement for single-molecule detection. To solve the above problem, Li and coworkers[74,75] proposed and experimentally demonstrated a plasmonic spiral tip for efficient transfer and focusing of input light. The high-transfer efficiency enabled by the spiral tip provides an additional pathway to increase the detection sensitivity toward single-molecule SERS. The theoretical design of the plasmonic spiral tip is shown in Fig. 2(e). By making use of the spiral design, the mirror symmetry of the plasmonic tip is broken, avoiding the destructive interference of the coupled surface plasmon polaritons at the apex of the tip. Based on the theoretical design, they first fabricated the template of the spiral tip using three-dimensional (3-D) direct laser writing, and then coated a uniform gold film with a thickness of 100 nm on the surface of the template via the magnetron sputtering technique. The SEM image of the fabricated plasmonic spiral tip is shown in the left panel of Fig. 2(f). The fabricated plasmonic spiral tip exhibits excellent focusing performance. A bright hot spot independent of the polarization of the input light is observed at the apex of the spiral tip as shown in the right panel of Fig. 2(f), indicating a high optical flux. Compared with the conventional plasmonic sharp tips with extreme pursuit of high electric-field enhancement, the plasmonic spiral tip opens up a new avenue toward single-molecule SERS.

3.1.3 Plasmonic complex nanostructures

Plasmonic complex nanostructures based on new physics and novel nanofabrication techniques have recently emerged as a new strategy for single-molecule SERS. Compared with plasmonic simple nanostructures, such as the nanogaps and sharp tips introduced above, the plasmonic complex nanostructures enable versatile functions and extraordinary optical properties to improve the experimental conditions for single-molecule SERS. Improving the experimental conditions of SERS measurement, such as increasing transfer efficiency of input light to hotspots and collection efficiency of Raman signals, can be another promising alternative for enhancing the sensitivity of SERS measurement. Several classical plasmonic complex nanostructures that enable improved experimental conditions for SERS measurement will be introduced in this section.

In 2013, Lin et al. proposed and experimentally demonstrated a complex SERS substrate with the function of electrostatic precipitation for effective localized collection and identification of molecules.[76] The schematic diagram of the SERS substrate comprising of plasmonic complex nanostructures is shown in Fig. 3(a). By applying an external biased voltage to the substrate, the electrostatic precipitation can be introduced into the substrate to increase collection efficiency of target molecules. A charged photoresist layer with circular openings as shown in the inset SEM image of Fig. 3(a) was fabricated for localizing charged molecules to further increase the collection efficiency of the target molecules. Compared with the identical nanostructured SERS substrate without the function of electrostatic precipitation, the sensitivity of the proposed complex SERS substrate is improved by two orders of magnitude as shown in Fig. 3(b). The proposed complex SERS substrate with the function of electrostatic precipitation indicates that increasing the collection efficiency of molecules on the substrate is a promising method to enhance the sensitivity of SERS measurement. Such a strategy also increases adsorptivity of molecules on the SERS substrate, which may also be applied to single-molecule SERS to decrease the SERS intensity fluctuation and increase the reproducibility of SERS measurement.[76]

Chen et al. utilized a plasmonic complex nanostructure consisting of a plasmonic nanoslit, a cavity, and two Bragg-mirror gratings to achieve single-molecule SERS.[77] The schematic diagram of the entire device is shown in Fig. 3(c). The cavity is able to efficiently couple the incident light into surface plasmon polaritons and guide them into the nanoslit, which provides an efficient transfer pathway for the incident light from the light source to the hotspot. The two Bragg-mirror gratings are used to reflect surface plasmon polaritons back to the nanoslit, further increasing the transfer efficiency. By making use of such a plasmonic complex nanostructure, extremely high electromagnetic enhancement is achieved in the nanoslit, which enables a high sensitivity up to the single-molecule level. In addition, a bias voltage is applied to the SERS substrate to attract negatively charged DNA molecules to pass through the nanoslit for SERS measurement. The bi-analyte approach was also used to experimentally verify the capability of the complex nanostructure for single-molecule detection, which is shown in Fig. 3(d). The proposed plasmonic complex nanostructure indicates that realization of high transfer efficiency of incident light from the far-field to the near-field can be a promising strategy for single-molecule SERS.[77]

Also Mao et al.[78] utilized a plasmonic complex nanostructure designed by transformation optics to achieve broadband enhancement of hotspots in both magnitude and volume for single-molecule SERS. The schematic diagram of the proposed plasmonic complex nanostructure, that is, a silver nanoparticle on a warped gold substrate, is shown in the inset of Fig. 3(e). The warped substrate is designed using transformation optics, which achieves an immense enhancement to form a larger and brighter hotspot as shown in Fig. 3(e). Compared with a silver nanoparticle on a flat gold substrate, an additional threefold enhancement for electric field is realized, enabling a much higher sensitivity. By employing such a plasmonic complex nanostructure, a Raman enhancement factor up to $\sim 10^9$ was experimentally realized, which is applicable for single-molecule detection. A bianalyte experiment was also conducted to verify the capability of the proposed plasmonic complex nanostructure for single-molecule detection, which is shown in Fig. 3(f).

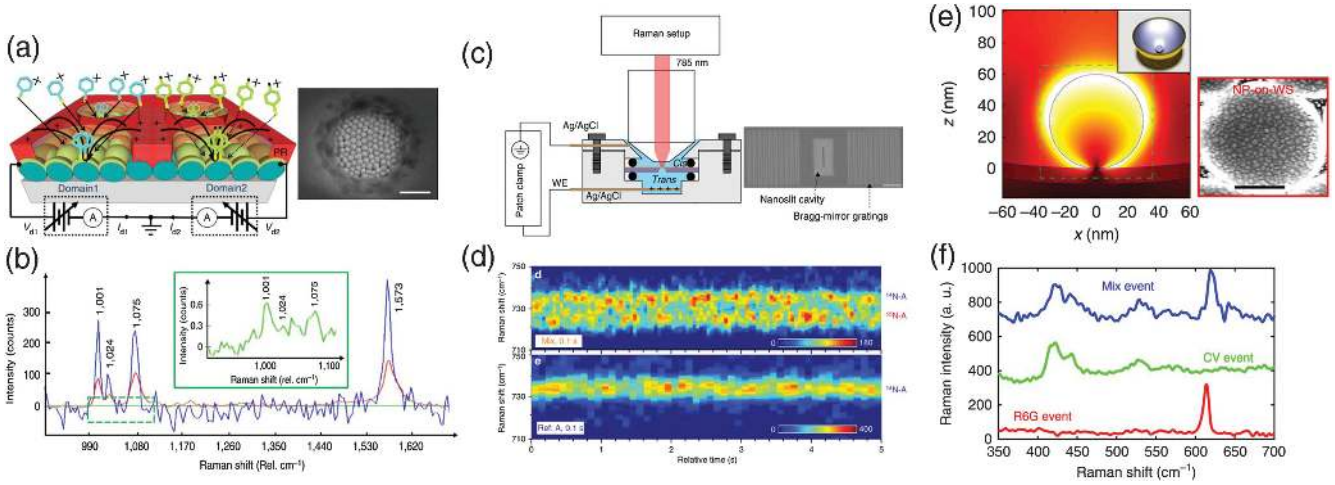

Fig. 3 Plasmonic complex nanostructures for single-molecule SERS. (a) Concept of a complex SERS substrate with the function of electrostatic precipitation for effective localized collection and identification of molecules. The inset is the scanning electron microscope image of the SERS substrate. (b) Raman intensity on the biased substrates is increased by a factor of 615.[76] (c) Schematic diagram of the setup for nanoslit SERS. The nanoslit chip is sealed in a flow cell, which separates the electrolyte solution into two compartments. The top chamber can accommodate a water-immersion objective lens. A 785-nm laser with 8 mW is focused on the gold nanoslit. Axon patch 200B amplifier is used to apply the transmembrane voltages and monitor the ionic currents between two Ag/AgCl electrodes. The inset shows a top-view SEM image of the nanoslit structure, consisting of an inverted prism nanoslit cavity with Bragg-mirror gratings. The scale bar is 1 μm. (d) The contour maps of SERS of a typical asynchronous blinking of the mixed isotopic adenines (top panel) and a typical fluctuation of the single adenine (bottom) recorded in 5 s, respectively, in single-molecule sensing.[77] (e) 3-D finite-difference time-domain simulations for a Ag nanoparticle on a warped Au substrate. A prominent field enhancement is demonstrated due to the effective gradient of permittivity. The right panel shows the SEM image of the substrate where the scale bar is 500 nm. (f) Typical spectra for bianalyte analysis.[78] Figures reprinted with permission: (a) and (b) Ref. 76, © 2013 by the Nature Publishing Group; (c) and (d) Ref. 77, © 2018 by the Nature Publishing Group; and (e) and (f) Ref. 78, © 2018 by the Nature Publishing Group.

The proposed nanostructure indicates that developing SERS substrates based on new physics is another alternative for single-molecule SERS.[78]

3.1.4 *Plasmonic substrates that enable delivery of single molecules to hotspots*

The delivery and stability of a single molecule at a hotspot for different environments is also a critical issue for single-molecule SERS. One of the most commonly used methods for an air-borne or a solution environment is to employ Langmuir–Blodgett monolayers as they are capable of controlling where and how the detected molecules are distributed.[45] The regular distribution provides the possibility of delivering one single molecule to one single hotspot on average when the concentration of the detected molecules is decreased to the single-molecule level. The method used for a vacuum environment is to utilize TERS. The hotspot generated by the tip of the TERS system is mechanically manipulated to approach a single molecule prefixed on a substrate.[73] In 2016, a new method called slippery liquid-infused porous SERS was demonstrated for a solution environment that enables detection of molecules present in solid, liquid, and air phases at the single-molecule level.[79] The method harnesses a slippery, omniphobic substrate that enables the complete concentration of molecules and SERS substrates (e.g., Au nanoparticles) within an evaporating liquid droplet to enrich and deliver molecules into the hotspot areas of the SERS substrates.

3.2 *Chemical Enhancement*

Chemical enhancement as another commonly applied strategy for SERS is also applicable for single-molecule SERS. Compared with electromagnetic enhancement, chemical enhancement achieves a relatively low enhancement factor up to 10^7.[25] Although single-molecule SERS enabled by chemical enhancement alone has not been demonstrated, chemical enhancement can definitely be employed as complementary to the electromagnetic enhancement for single-molecule SERS, or to relax the rigorous requirement on electromagnetic enhancement to fuel broad applications. Furthermore, chemical enhancement enables exploration of a variety of materials, such as semiconducting metal oxides and 2-D materials, as SERS substrates, thus providing more options for single-molecule SERS under various physical and chemical environments.

Chemical enhancement enhances Raman signal intensity by providing additional pathways of charge-transfer resonance.[80] A typical energy diagram of a substrate-molecule hybrid system consisting of a metal SERS substrate and an adsorbed molecule

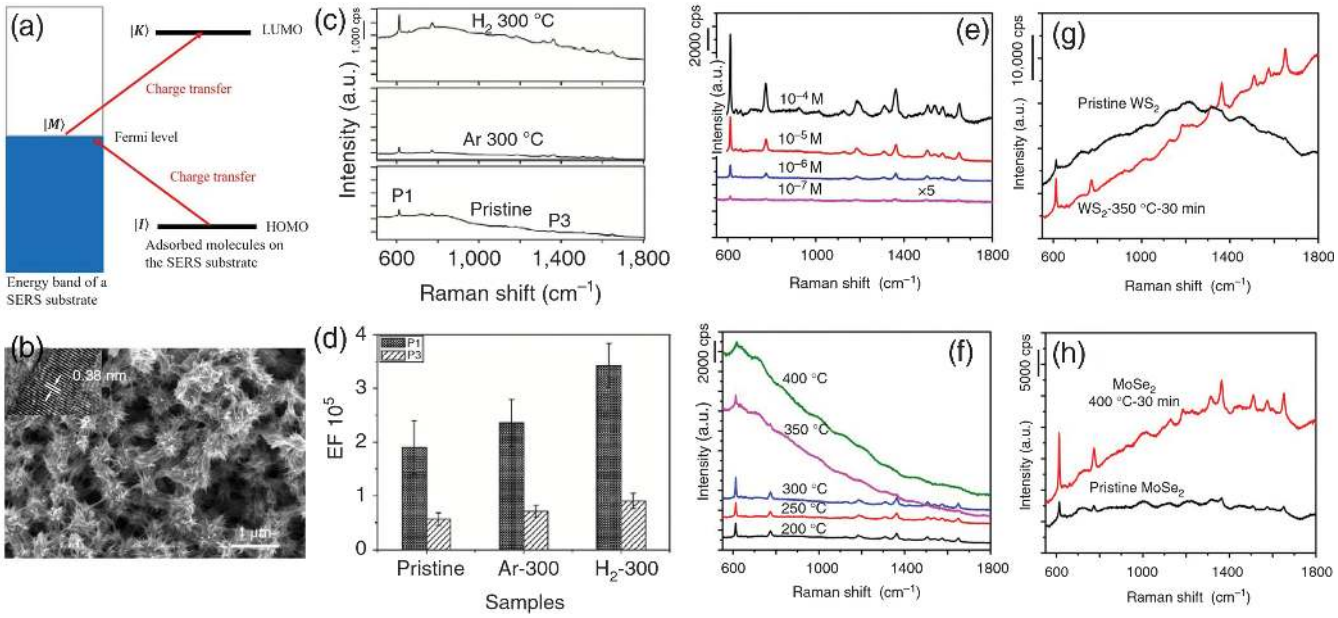

Fig. 4 Chemical enhancement for single-molecule SERS. (a) A typical energy diagram of a substrate–molecule hybrid system consisting of a metal SERS substrate and an adsorbed molecule.[80] (b) Scanning electron microscopy image for $W_{18}O_{49}$ sample. Inset in (b): high-resolution transmission electron microscopy image on one single nanowire illustrating clear lattice fringe of 0.38 nm, which suggested that the nanowire growth was along the [010] direction. (c) Improved SERS properties of $W_{18}O_{49}$ samples after Ar/H_2 annealing treatment. Raman signals of R6G molecule on pristine $W_{18}O_{49}$ and the samples after annealing treatment (in Ar/H_2 for 1 h). The tested concentration of R6G was 1×10^{-6} M. (d) A comparison of Raman EF for the two respective vibration modes P1 and P3. Data reported in this histogram resulted from Raman spectra acquired over 30 different regions per sample and provide an indication of the EF for each Raman mode. The H_2-treated sample shows the greatest enhancement at band P1, the EF for which was evaluated to be 3.4×10^5.[8] (e) Raman spectra collected for oxygen-incorporated MoS_2 sample annealed for 40 min at four different concentrations, 10^{-4}, 10^{-5}, 10^{-6}, and 10^{-7} M, suggesting the detection limit was as low as 10^{-7} M. (f) SERS spectra on the oxygen-incorporated MoS_2 samples with different annealing temperatures. (g) and (h) SERS spectra of R6G on a series of other semiconductor materials WS_2 and $MoSe_2$ respectively.[23] Figures reprinted with permission: (a) and (b) Ref. 80, © 1986 by the American Institute of Physics; (c) and (d) Ref. 8, © 2015 by the Nature Publishing Group; (e)–(h) Ref. 23, © 2015 by the Nature Publishing Group.

is shown in Fig. 4(a). The Raman intensity, I_R, is proportional to the product of the intensity of incident light, I_L, and the square of the Raman polarizability, $\alpha_{\sigma\rho}$, of the molecule:

$$I_R \propto I_L |\alpha_{\sigma\rho}|^2. \tag{3}$$

The Raman polarizability $\alpha_{\sigma\rho}$, which is composed of three terms can be expressed as

$$\alpha_{\sigma\rho} = A + B + C, \tag{4}$$

where

$$A = \sum_{K\neq I}\sum_{k}\left[\frac{M^{\sigma}_{KI}(Q_0)M^{\rho}_{KI}(Q_0)}{\hbar(\omega_{KI}-\omega)} + \frac{M^{\rho}_{KI}(Q_0)M^{\sigma}_{KI}(Q_0)}{\hbar(\omega_{KI}+\omega)}\right]\langle i|k\rangle\langle k|f\rangle, \tag{5}$$

$$B = -(2/\hbar^2)\sum_{K\neq I}\sum_{M<K}[M^{\sigma}_{KI}M^{\rho}_{MI} + M^{\rho}_{KI}M^{\sigma}_{MI}]\frac{(\omega_{KI}\omega_{MI}+\omega^2)h_{KM}\langle i|Q|f\rangle}{(\omega^2_{KI}-\omega^2)(\omega^2_{MI}-\omega^2)}, \tag{6}$$

$$C = -(2/\hbar^2)\sum_{K\neq I}\sum_{M>I}[M^{\sigma}_{MK}M^{\rho}_{KI} + M^{\rho}_{MK}M^{\sigma}_{KI}]\frac{(\omega_{KI}\omega_{KM}+\omega^2)h_{IM}\langle i|Q|f\rangle}{(\omega^2_{KI}-\omega^2)(\omega^2_{KM}-\omega^2)}. \tag{7}$$

Here, M_{KI}, M_{MI}, and M_{MK} are the electronic transition moments between the states of $|K\rangle$ and $|I\rangle$, $|M\rangle$ and $|I\rangle$, as well as $|M\rangle$ and $|K\rangle$, respectively, as shown in Fig. 4(a). Q_0 is the nucleus coordinate. $|i\rangle$, $|k\rangle$, and $|f\rangle$ represent the initial state, excited state, and final state of the nucleus, respectively. h_{KM}

and h_{IM} stand for the vibronic couplings of the metal substrate to the excited molecular state as well as to the ground state, respectively. ω is the frequency of the excitation laser. ω_{KI}, ω_{MI}, and ω_{KM} are the molecular transition frequencies between states of $|K\rangle$ and $|I\rangle$, $|M\rangle$ and $|I\rangle$, as well as $|M\rangle$ and $|K\rangle$, respectively. Therefore, term B represents the molecule-to-substrate charge transfer from the highest occupied molecular orbital to the Fermi level of the substrate. Similarly, term C represents the substrate-to-molecule charge transfer from the Fermi level of the substrate to the lowest unoccupied molecular orbital of the molecule. It can be inferred from Eq. (6) that the enhancement for term B comes from the resonance denominator, $\omega_{MI}^2 - \omega^2$, when ω is close enough to ω_{MI}. Similarly, term C is enhanced when ω is close to ω_{KM}. With the resonant enhancement of term B or term C, the Raman polarizability of the molecule $\alpha_{\sigma\rho}$ is also enhanced, resulting in the dramatic enhancement of the Raman intensity I_{R}.

Through chemical enhancement, a series of nonmetal substrates with high Raman enhancement capabilities were developed by material engineering. Cong et al. demonstrated a Raman enhancement factor of 3.4×10^5 with urchin-like $W_{18}O_{49}$ substrate [Fig. 4(b)], in which the oxygen vacancies contributed significantly to the chemical enhancement of Raman intensity.[8] Specifically, as shown in Figs. 4(c) and 4(d), the additional oxygen vacancies in $W_{18}O_{49}$ created with Ar/H_2 annealing treatment enriched the surface states of the material, which provided magnified affinity for the adsorbent–adsorbate interaction and enhanced the Raman signal through charge-transfer resonance. The highest enhancement factor of 3.4×10^5 was experimentally realized by utilizing oxygen vacancies. On the contrary, by incorporating oxygen into MoS_2 substrate, Cong et al. also achieved high chemical enhancement with a SERS detection limit of rhodamine 6G molecules down to the concentration of 10^{-7} M (1M = 1 mol/L) [Figs. 4(e) and 4(f)].[23] Some other substrates, including WS_2 and $MoSe_2$ [Figs. 4(g) and 4(h)], were also successfully equipped with chemical enhancement for SERS by the oxygen incorporation approach. The chemical enhancement significantly broadens the potential material platform for SERS, which is expected to promote single-molecule SERS by combination with electromagnetic enhancement.

3.3 Resonance Enhancement

Resonance enhancement is a classic and well-studied strategy for enhancing the weak Raman scattering signals. Apart from its wide employment for measuring the spontaneous Raman spectra of various molecules in solid state or liquid solutions, attempts have been made to utilize resonance enhancement in SERS measurement. To date, the Raman enhancement factors contributed by resonance enhancement have been found to be between 10^4 and 10^6, which are unable to facilitate single-molecule SERS alone but still provide considerable enhancement effect. More importantly, achieving resonance enhancement is readily feasible regardless of the substrate since it directly results from the interaction between the excitation photon and the probed molecule. Therefore, similar to chemical enhancement, resonance enhancement can be used in parallel with other strategies to further amplify the Raman signals.

The mechanism of resonance enhancement is relatively simple and straightforward compared with the strategies above, as the substrate is not involved. Typically, resonance enhancement occurs when the energy of the incident photon is close to the energy required for electronic transition between states of $|K\rangle$ and $|\mathrm{I}\rangle$, in the probed molecule as shown in Fig. 4(a). Under the resonance condition, the term A in Eq. (5) is drastically enhanced through the resonance denominator, $\omega_{KI}^2 - \omega^2$, when ω is close to ω_{KI}. Similar to the chemical enhancement, the molecular Raman polarizability, $\alpha_{\sigma\rho}$, is also enhanced, leading to the enhancement of the Raman intensity I_{R}.

Resonance enhancement has long been employed for SERS by virtue of its great convenience. Hildebrandt et al. studied the surface-enhanced resonance Raman scattering (SERRS) of rhodamine 6G adsorbed on colloidal silver.[81] By virtue of the high detection sensitivity enabled by resonance enhancement, they were able to distinguish the two different kinds of adsorption sites on the surface of the silver particles with different enhancement mechanisms. Hildebrandt et al. also investigated the SERRS of cytochrome c (cyt) at room and low temperatures.[82] From the SERRS spectra of cyt^{3+} adsorbed on Ag glycerol sol at different temperatures, they demonstrated the adsorption-induced partial transition of cyt^{3+} molecules from the low-spin (LS) state to the high-spin (HS) state. As one of the important Raman enhancement strategies, resonance enhancement offers alternative or complementary chances for realizing single-molecule SERS.

3.4 Other Potential Strategies

Besides the above mature strategies, new strategies need to be continuously proposed and developed to promote the advance of single-molecule SERS. Potential new strategies may come from new understanding and interpretation of single-molecule SERS, as the mechanism of single-molecule SERS is still not completely understood. For example, as we have introduced in Sec. 3.1.2, the state-of-the-art TERS enables not only single-molecule sensitivity but also subnanometer spatial resolution.[83–89] However, numerical simulation based on the conventional SERS theory indicates that the hotspot size generated by the plasmonic sharp tip used in the experiment is still in the order of 10 nm, as shown in Fig. 5(a), which is much larger than the experimentally realized spatial resolution.[90] How a 10-nm hotspot enables subnanometer spatial resolution has aroused great interest and discussion.

To interpret this puzzling question, Li and coworkers theoretically investigated it and found that Rayleigh scattering of the molecule that is previously ignored in conventional SERS theory plays an unexpectedly critical role, which may be one of the main contributors to the subnanometer spatial resolution.[90] With the assist of multiple Rayleigh scattering, a super hotspot with a shrunken size as shown in Fig. 5(b) is generated for achieving a high spatial resolution. Based on this discovery, they proposed an extended Raman theory to amend the conventional Raman theory. In conventional Raman theory, the influence of the molecule on the hotspot excited by the incident light is totally ignored, as shown in Figs. 5(c) and 5(d). In the extended Raman theory, as shown in Figs. 5(e) and 5(f), they took the influence of the molecule on its surrounding electromagnetic background into consideration. When the molecule size is comparable with the nanogap size and the distance to the plasmonic sharp tip, its Rayleigh scattering within the nanogap will respond and modify the localized electric field of both the excitation light and the Stokes (anti-Stokes) radiation light. This response and modification is called the electromagnetic

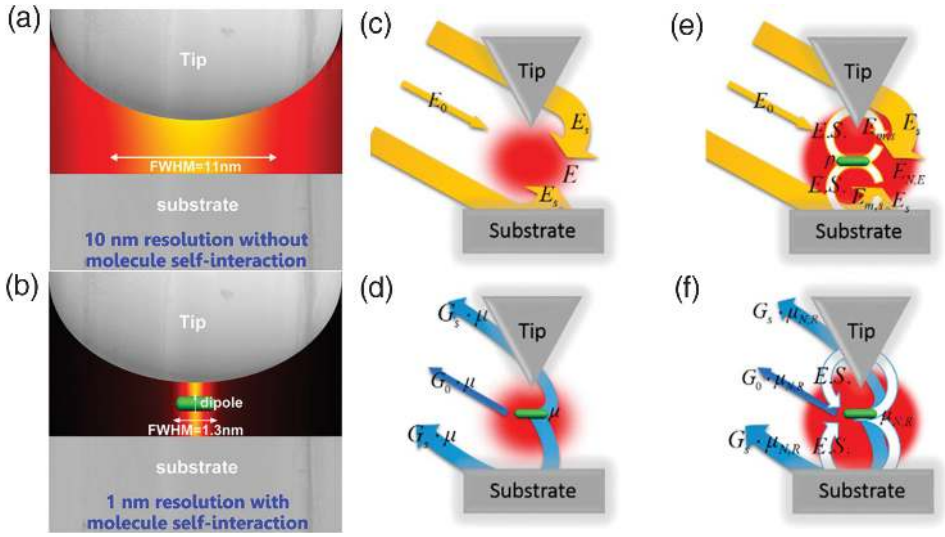

Fig. 5 Potential strategy for single-molecule SERS enabled by Rayleigh scattering-assisted Raman enhancement theory. Schematic configuration of TERS system used for Raman mapping of molecule (a) with and (b) without molecule selfinteraction. (c) The excitation process in classical Raman physics, where the incident light is scattered by the Ag tip–substrate nanogap to form highly localized plasmonic gap mode with greatly enhanced electric field intensity. E_0 and E_s (yellow arrows) are the incident and scattering electric fields, summing up to the local field E. (d) The radiation process in classical Raman physics, where the Raman signal emitted by the molecule is scattered by the Ag–substrate gap to have greatly enhanced far-field intensity. $G_0 \cdot \mu$ and $G_s \cdot \mu$ (blue arrows) are the direct Raman radiation of molecule (described by the dipole moment μ) and greatly enhanced scattering Raman radiation by the tip–substrate nanogap, where G_0 and G_s are free-space and scattering dyadic Green's function. (e) The excitation process in the extended Raman physics considering the molecule selfinteraction with the Ag tip–substrate gap through multiple elastic scattering (white arrows, abbreviated by *E.S.*) for the incident light. $E_{m,s}$ is the modified excitation field due to the *E.S.* mechanism and p is the induced dipole moment. (f) The radiation process in the extended Raman physics when considering the molecule selfinteraction. The multiple *E.S.* mechanism (white arrows) strongly modifies the molecule dipole moment to a value $\mu_{N,R}$.[90] (a)–(f) Figures reprinted with permission from Ref. 90, © 1986 by the American Chemical Society.

selfinteraction process of the molecule, which is characterized through Raman polarizability of the molecule and the induced dipole moment. The effective localized electric field of the incident light that includes the influence of the Rayleigh scattering of the molecule will be determined selfconsistently as

$$E_{\mathrm{N,E}}(r_0,\omega) = g(r_0,\omega)\cdot E(r_0,\omega), \tag{8}$$

where $g(r_0,\omega)$ is the selfinteraction modification factor. Similar to Eq. (1), the extended Raman enhancement factor, which should be also proportional to the fourth power of the local field enhancement, is expressed as

$$\begin{aligned} G_{\mathrm{S}}(r_0) &= |E_{\mathrm{N.E}}(r_0,\omega)|^4/|E_0(r_0,\omega)|^4 \\ &= g^4(r_0,\omega)|E(r_0,\omega)|^4/|E_0(r_0,\omega)|^4. \end{aligned} \tag{9}$$

The corresponding enhanced Raman intensity is modified as

$$\begin{aligned} I(\omega_{\mathrm{R}}) &= AG_{\mathrm{S}}(r_0)|\alpha(\omega_{\mathrm{R}},\omega)|^2 I_0(r_0,\omega) \\ &= AI_0(r_0,\omega)|\alpha(\omega_{\mathrm{R}},\omega)|^2 \times g^4(r_0,\omega) \\ &\quad \times |E(r_0,\omega)|^4/|E_0(r_0,\omega)|^4. \end{aligned} \tag{10}$$

Compared with the conventional Raman enhancement factor in Eqs. (1) and (2), there is a supplemental term equal to the fourth power of the near-field selfinteraction modification factor, and thus this theory involves plenty of new physics. The most prominent is that the molecule is not only driven by the plasmon-enhanced local electric field participating in both the Raman excitation and radiation processes, but also changes its plasmonic environment via elastic Rayleigh scattering-assisted selfinteraction. Such a change in the plasmonic environment will counteract to change the local electromagnetic field around the molecule and modify the Raman excitation and radiation processes significantly. The extended Raman theory provides potential strategies for single-molecule SERS. For example, high-performance SERS substrates with optimization of Rayleigh scattering of single molecules with specific orientations may be proposed and experimentally realized in future.

4 Applications of Single-Molecule SERS

4.1 Process Monitoring of Chemical Catalysis

The central issue of catalytic chemistry is to understand how single molecules interact with each other, which provides us with the possibility to precisely design and control various chemical

reactions that are critical to our lives.[91–95] Elucidating the molecular mechanisms of chemical reactions requires the observation of single-molecule behavior at subnanometer scale, which is beyond the detection limit of most analytical tools. Fortunately, by virtue of its extremely high sensitivity, single-molecule SERS enables the real-time tracking of molecules undergoing chemical reactions. In addition, the surface plasmons in subnanometer scale cavities generate hot charge carriers that can catalyze chemical reactions or induce redox processes of molecules located at the hotspots.[29]

Using single-molecule SERS, Zhang et al. studied the concentration-dependent intermolecular and intramolecular reactions catalyzed by surface plasmons on gold dimers.[29] By analyzing the single-molecule SERS spectra of *p*-nitrothiophenol (*p*NTP) molecules, they found that *p*NTP molecules tended to dimerize into 4,4-dimercaptoazobenzene (DMAB) at higher concentrations [Figs. 6(a) and 6(b)] while *p*NTP exclusively reacted to thiophenol (TP) at or close to the single-molecule level [Fig. 6(c)] where intermolecular reactions could not occur. Nijs et al. employed single-molecule SERS to study the hot-electron-induced redox processes in single aromatic molecules that are located at the nanocavity with a nanoparticle-on-mirror configuration, as shown in Fig. 6(d).[30] Specifically, they observed the change in SERS spectra of a single molecule during a time period of 0.9 s, as shown in Fig. 6(e), showing the occurrence of reduction and oxidation processes at the single-molecule level. In addition to reactive molecules, single-molecule SERS can also be applied to study the catalytic activity of nanoparticles. Recently, Zhang et al. demonstrated the direct SERS tracking of the reduction of a 4-nitrothiophenol (4-NTP) catalyzed by a single 13-nm small gold nanoparticle (S-GNP) in aqueous solution.[31] Based on a configuration composed of a large gold nanoparticle (L-GNP) and an S-GNP [Fig. 6(f)], the time-resolved single-molecule SERS spectra [Fig. 6(g)] were recorded to demonstrate the borohydride addition during the reaction process. It can be seen from the above examples that single-molecule SERS has become a powerful tool for process monitoring of chemical catalysis at the single-molecule level.

4.2 Imaging of Vibrational Modes

Visualizing single molecules provides the most straightforward answers to a lot of chemical and biological questions with unprecedented detail. Atomic force microscopy (AFM) is commonly used to image the morphology of single molecules but fails to recognize chemical information of single molecules. In contrast, single-molecule SERS probes the vibrational modes of single molecules, which contain rich information of their chemical bonds and functional groups. With its chemical specificity, single-molecule SERS opens up a new window for high-content vibrational imaging of single molecules.

In 2015, by detecting vibrational fingerprints with an STM-controlled TERS, as shown in Fig. 7(a), Jiang et al. successfully distinguished two adjacent molecules with similar morphologies, zinc-5,10,15,20-tetraphenyl-porphyrin (ZnTPP) and meso-tetrakis (3,5-di-tertiarybutyl-phenyl)-porphyrin (H_2TBPP), which are indistinguishable with AFM.[32] The measured Raman spectra of the two molecules to be distinguished, as shown in Fig. 7(b), exhibit obvious distinction. To further enhance the signal-to-noise ratio of the measured single-molecule Raman spectra for subnanometer-resolved vibrational imaging, Jiang et al. utilized multivariate analysis based on STM images and TERS images [Figs. 7(c)–7(g)] to achieve identification of single ZnTPP and H_2TBPP molecules.[33] In addition, instead of directly detecting TERS signals of the probed molecules for imaging, electrostatic fields of single molecules can also be mapped with an intermediate single-molecule probe. With TERS-relayed molecular force microscopy (TERS-mfm), Lee et al. successfully imaged the distribution of electrostatic fields of single molecules.[34] As shown in Fig. 7(h), TERS was utilized to measure the vibrational modes of a tip-attached single CO molecule, which was perturbed by the electrostatic fields of the probed molecule. The reconstructed distributions of electrostatic fields of cobalt(II)-tetraphenylporphyrin (CoTPP) and zinc(II)-etioporphyrin (ZnEtio) molecules on Au(111) substrate are shown in Figs. 7(i) and 7(j). By virtue of its high flexibility and submolecular level spatial resolution, single-molecule SERS is a promising technique for various high-content chemical imaging.

In addition, imaging vibrational modes of molecules can retrospectively help interpret the nature of SERS substrates. To elucidate the time-dependent signal fluctuation in single-molecule SERS, Lindquist et al. studied the hotspot dynamics on single nanoparticles by high-speed single-molecule SERS imaging.[40] Surprisingly, the surface of a fully functionalized SiO_2@Ag nanoparticle remains dark more than 98% during the measurement, suggesting that the hotspots are formed transiently due to the random reconstruction of the metal surface. By further analyzing the influence of several factors, such as temperature and excitation wavelength, the authors concluded that the signal fluctuation mainly results from the transient formation of hotspots driven by the random reconstruction of the metal surface. The work provides a promising method to investigate the fast dynamic properties of single-molecule SERS hotspots.

4.3 Observation of Charge Transfer in Nanoelectronics

Nanoelectronic devices are of essential importance to advanced electronic products, such as central processing units, electronic memory storages, and optoelectronic devices. Molecular nanoelectronics that utilize single molecules as active components are capable of realizing information systems with extremely high performance and low power consumption. Studying molecular charge transfer provides insights into the design and fabrication of molecular nanoelectronic devices. Similar to the difficulties in investigating single molecules, conventional methods are usually unable to probe such subtle and dynamic phenomena due to their limited sensitivities. Single-molecule SERS, which is highly sensitive to the variations in molecular charge transfer processes, has great potential to fulfill the requirements of characterizing molecular nanoelectronic devices.

Li et al. studied the voltage-driven tuning of vibrational mode energies of single molecules.[35] By applying different bias voltages to the C_{60} molecules in gold junctions [Fig. 8(a)], they observed shifts in molecular vibrational modes, which presumably resulted from the addition of electronic charge to the molecule, instead of simple Stark effect, through the analysis of single-molecule SERS spectra [Figs. 8(b) and 8(c)]. In contrast, Han et al. used single-molecule SERS to directly investigate the mechanisms of charge transfer.[36] For the first time, they achieved the assessment of the contribution of SPR to charge transfer by tuning the surface plasmon absorption of Au nanorods with a series of excitation wavelengths [Figs. 8(d) and 8(e)]. They also proposed the physical mechanisms of plasmon-assisted charge transfer in such semiconductor/organic molecule/Au

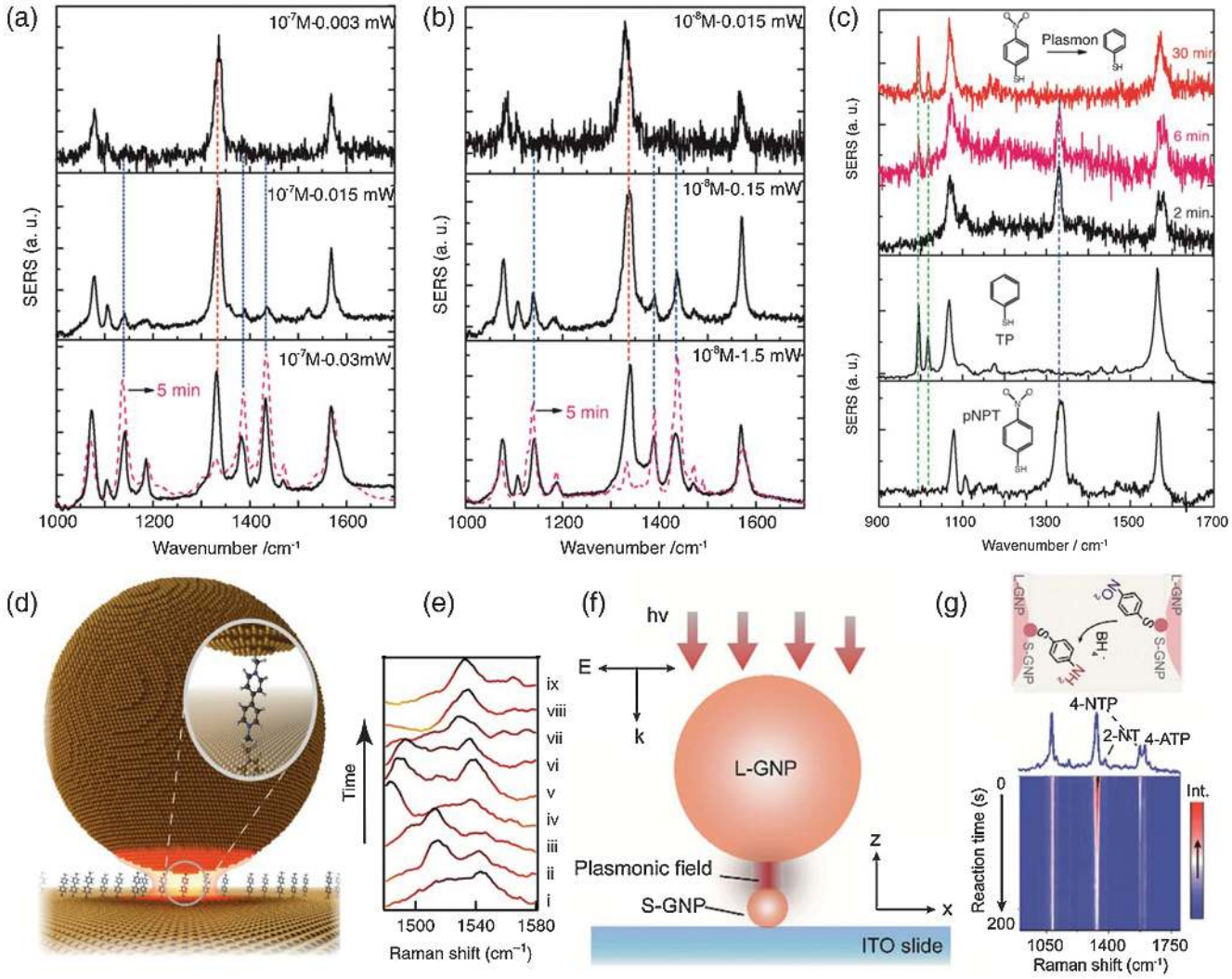

Fig. 6 Process monitoring of chemical catalysis by single-molecule SERS. (a) SERS spectra of 10^{-7} M *p*NTP excited at 3, 15, and 30 mW laser power, respectively. (b) SERS spectra of 10^{-8} M *p*NTP excited at 0.015, 0.15, and 1.5 mW laser power, respectively. (c) From top to bottom: Time-dependent SERS spectra of reacting *p*NTP ($c = 10^{-9}$ M) at 3 mW laser at 2, 6, and 30 min; normal SERS spectra of TP and *p*NTP, respectively.[29] (d) Selfassembled 80-nm nanoparticle-on-mirror geometry used to elicit field enhancements required for single-molecule spectroscopy. (e) Short (0.9 s) segment from NPoM time scan showing the reduction and oxidation processes.[30] (f) Schematic diagram showing the configuration of an L-GNP/S-GNP dimer linked with 1,6-hexanedithiol. (g) (top) Schematic illustration showing the S-GNP catalyzed reduction of 4-NTP in the presence of borohydride. (bottom) Color-coded intensity map of time-dependent single-NP SERS spectra after borohydride addition, with a range of Raman shifts between 900 and 1800 cm^{-1} for a 1 s integration time, taken every 5 s at 638 nm.[31] Figures reprinted with permission: (a)–(c) Ref. 29, © 2015 by the Royal Society of Chemistry; (d) and (e) Ref. 30, © 2017 by the Nature Publishing Group; and (f) and (g) Ref. 31, © 2019 by the Royal Society of Chemistry.

assemblies [Fig. 8(f)]. Therefore, single-molecule SERS is highly expected to lead to fundamental breakthroughs in the field of nanoelectronics as it allows for the direct interrogation of charge transfer processes.

4.4 Combination with Other Techniques

Besides the stand-alone application of single-molecule SERS, single-molecule SERS has also been combined with some other techniques to create new tools for studying various phenomena at the single-molecule level. On the one hand, the combined techniques may either compensate for the intrinsic drawbacks of single-molecule SERS or provide tunable circumstances for single-molecule SERS measurement, thus enabling systematic investigation of single-molecule events. On the other hand, the single-molecule SERS can equip the combined techniques with ultrahigh sensitivity and high-content information of molecular vibration. For example, single-molecule SERS

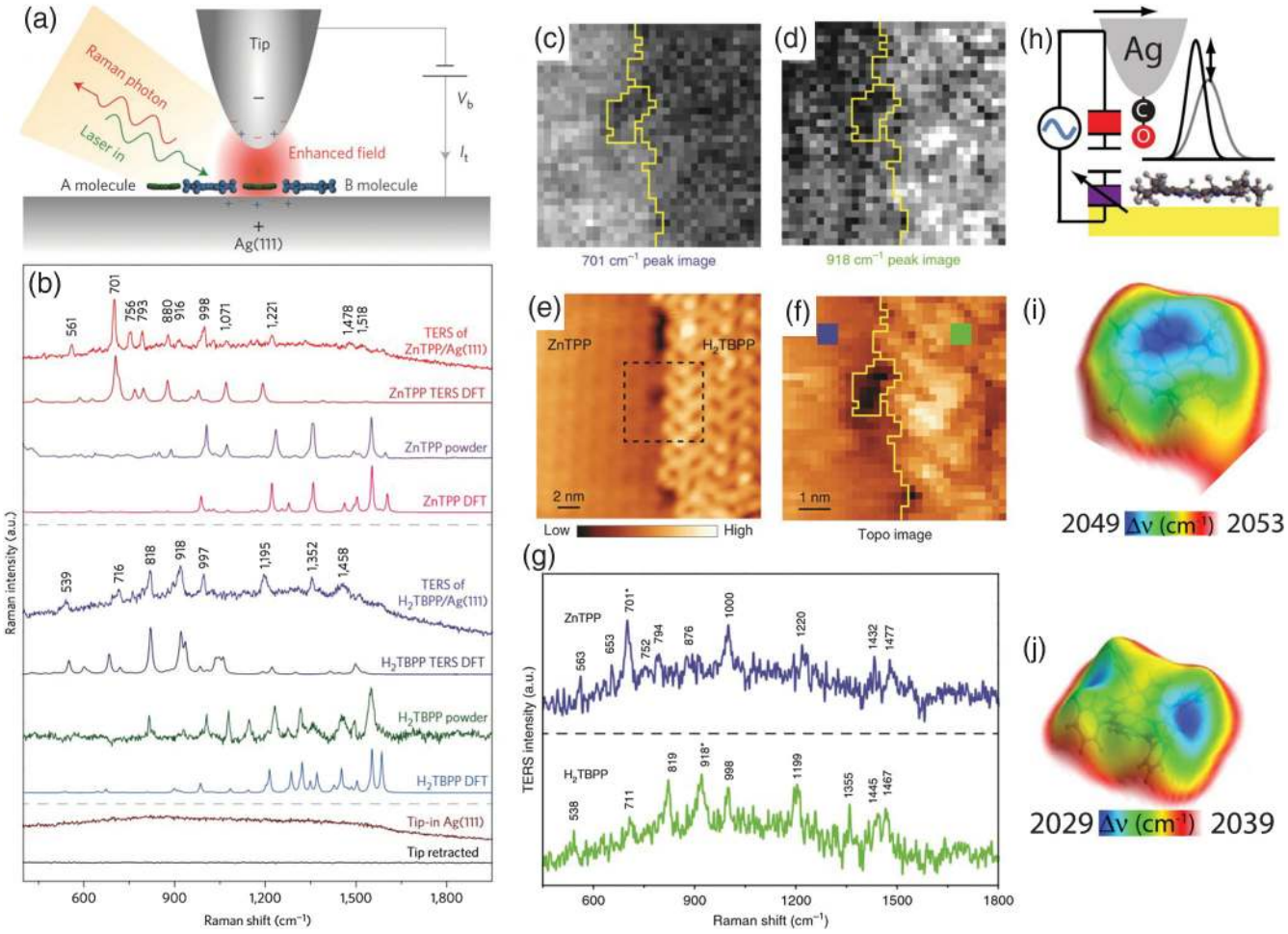

Fig. 7 Imaging of vibrational modes by single-molecule SERS. (a) Schematic of STM-controlled TERS in a confocal-type side-illumination configuration on Ag (111) using Ag tips. (b) TERS spectra acquired above ZnTPP or H_2TBPP molecular islands (0.1 V, 1 nA, 30 s). For comparison, powder Raman spectra and Raman spectra calculated via DFT are also shown. The brown spectrum was taken on bare Ag (111) (0.1 V, 1 nA, 30 s) and the black spectrum was measured on top of a molecular island but with the tip retracted 5 nm from the surface (0.1 V, 30 s).[32] (c), (d) TERS images reconstructed based on single-peak analysis for the Raman peaks at ~701 cm^{-1} (c, integrated over 687 to 736 cm^{-1}) and ~918 cm^{-1} (d, integrated over 890 to 959 cm^{-1}). (e) STM image of two adjacent porphyrin molecular domains (−1 V, 5 pA). (f) STM image simultaneously acquired during TERS imaging of the area denoted by the dashed square in (e) (–0.1 V, 1 nA, 7 nm × 7 nm, 32 × 32 pixels, 1 s per pixel). The boundary between the molecular domains is highlighted by a yellow line. (g) TERS spectra, averaged over the blue and green squares (3 × 3 pixels) shown in (f), extracted from the datacube for ZnTPP and H_2TBPP molecules, respectively.[33] (h) Diagram of the system to detect the distribution of the electrostatic fields of single molecules. (i) Electrostatic field surface obtained by color-coding the Stark on the STM CH topography. The common image size is 23 × 23 . The set point is 0.1 nA, 1.2 V. (j) Electrostatic field mapped on the isosurface of local density of states. The common image size is 27 × 27 . The set point is 0.1 nA, 1.2 V.[34] Figures reprinted with permission: (a) and (b) Ref. 32, © 2015 by the Nature Publishing Group; (c)–(g) Ref. 33, © 2017 by the Nature Publishing Group; (h)–(j) Ref. 34, © 2018 by the American Association for the Advancement of Science.

can be combined with electrochemical or mechanical techniques to monitor single-molecule chemical reactions. In this section, we will provide several examples of combination of single-molecule SERS with other techniques and discuss their potential applications.

In 2010, by integrating an electrochemical setup with single-molecule SERS [Fig. 9(a)], Cortes et al. tracked the redox processes of single molecules in a time-dependent manner and compared the SERS spectra of single- and many-molecule events.[96] Specifically, using the bianalyte method, they collected the

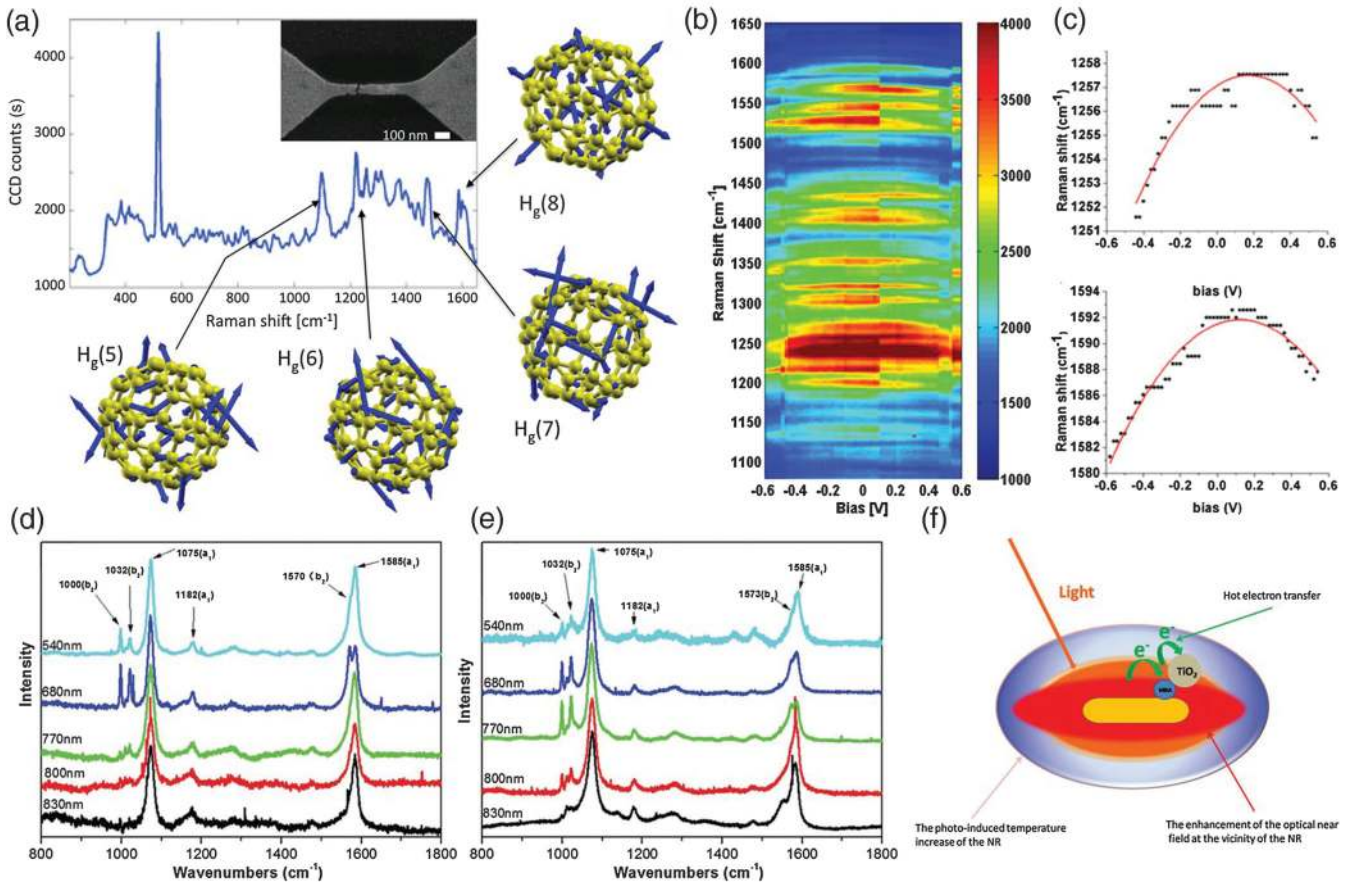

Fig. 8 Observation of charge transfer in nanoelectronics by single-molecule SERS. (a) Raman analysis of C_{60} in an electromigrated junction. (Main plot) Example of a SERS spectrum of C_{60} in an electromigrated junction. Surrounding diagrams illustrate examples of the complicated displacements associated with Raman-active modes, calculated for an isolated, symmetric, gas-phase molecule. Each such mode is fivefold degenerate in the absence of symmetry breaking. (Inset) Scanning electron microscopic image of an electromigrated junction. (b) Raman response of device 3 as a function of bias (x axis) and Raman shift (y axis). The sudden change in the intensity at around 0.1 V is the result of blinking. (c) Vibrational energy shift as a function of bias for three particular modes: 1258 and 1592 cm^{-1}. The discretized Raman shift data result from pixilation of the detector.[35] (d), (e) SERS spectra of 4-MBA in the different TiO_2–MBA–Au NR assemblies at excitation wavelengths of (d) 633 nm and (e) 785 nm. The numbers on the left side in each figure indicate the SP absorption peaks of the TiO_2–MBA–Au NR assemblies. (f) Main physical mechanisms involved in plasmon-assisted charge transfer.[36] Figures reprinted with permission: (a)–(c) Ref. 35, © 2014 by the National Academy of Sciences; (d)–(f) Ref. 36, © 2018 by the Royal Society of Chemistry.

SERS signals of rhodamine 6G (RH6G) and nile blue (NB) in an open-frame electrochemical cell. Using SERS intensity as a tag, they demonstrated that the single-molecule events differ from one molecule to another at the same position [Fig. 9(b)]. Also, as shown in Fig. 9(c), the behaviors of one molecule vary between two successive cycles. In addition, Zheng et al. combined mechanically controllable break junction (MCBJ) with single-molecule SERS to study the conductance discrepancy of benzene-1,4-dithiol (BDT).[97] As shown in Fig. 9(d), the single-molecule SERS and electric conductance of BDT molecules are measured in an MCBJ setup. By comparing the SERS spectra of BDT under different conditions [Fig. 9(e)], they clarified that the dimerization of BDT was responsible for the low conductance status before the junction break [Figs. 9(f) and 9(g)]. Besides, single-molecule SERS itself can also be improved by combination with other techniques. For example, Patra et al. demonstrated the reversible assembly of plasmonic nanoparticles for single-molecule SERS, which overcame the limitations of irreversible chemical aggregation.[98] Notably, as shown in Fig. 9(h), they applied a single evanescent-wave excitation beam to achieve the nanoparticle assembly and single-molecule SERS simultaneously. They also created interacting nanoparticle assemblies using two excitation beams [Fig. 9(i)]. To summarize, the combination of single-molecule SERS with other techniques significantly expands the application of conventional single-molecule SERS, which is expected to contribute to diverse applications, such as study of protein–protein interaction and design of molecular motors.

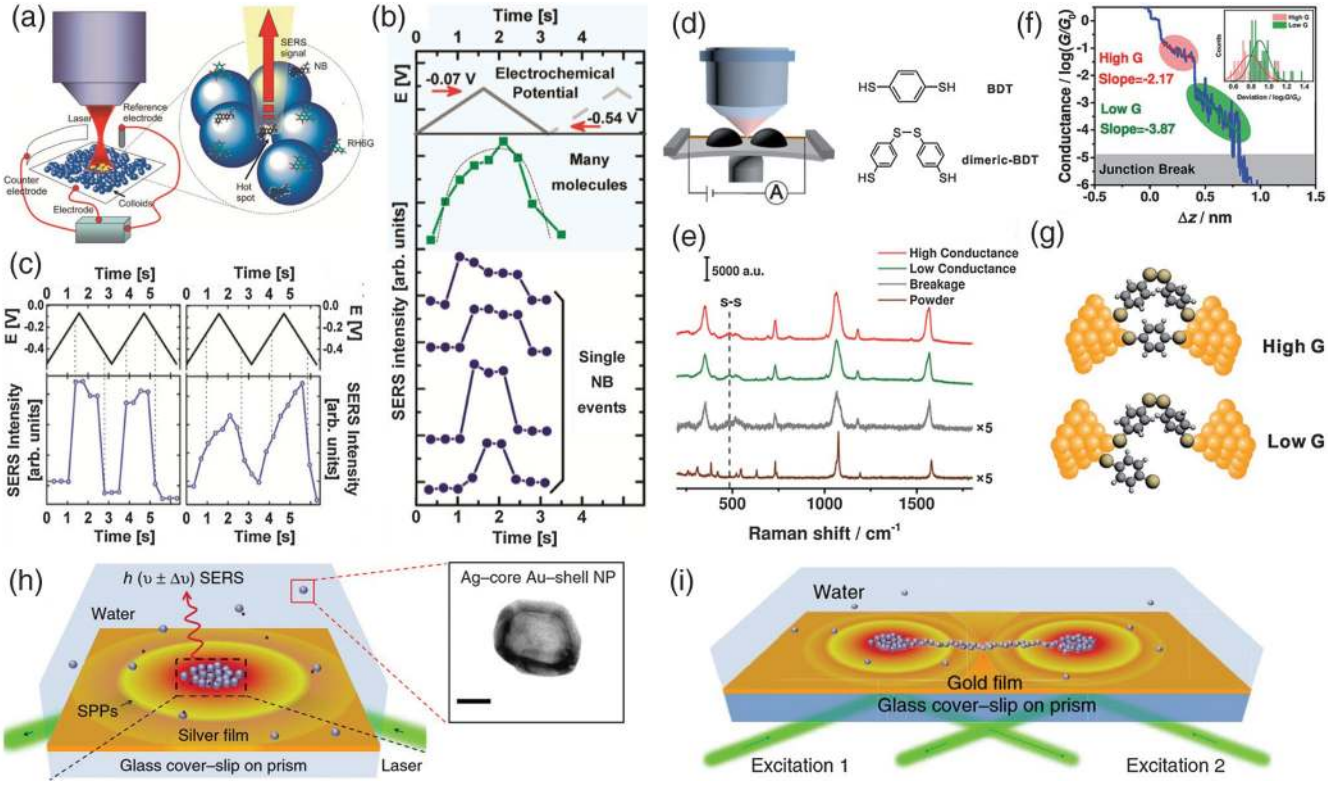

Fig. 9 Combination of single-molecule SERS with other techniques. (a) Ag colloids premixed with a suitable combination of bianalyte SERS partners (RH6G and NB at 2- to 5-nM concentration) are deposited on a working electrode (Ag) in an open-frame electrochemical cell (with a wide-area Pt counter electrode and a Ag/AgCl reference electrode). (b) Many molecule and SM-SERS intensity cases for NB. The varied durations of the signals in the "on" (oxidized) state reveal the different redox potentials for that particular molecule. (c) Variations in redox properties for two consecutive cycles, as determined from the SERS intensity of the 590 cm^{-1} peak of NB along two voltammetric cycles: single molecule; many molecules.[96] (d) Schematic of the MCBJ-SERS setup and the molecular structures of BDT and dimeric-BDT. (e) SERS spectra collected when the molecular junction was mechanically controlled at the regimes of high conductance (red), low conductance (green), and breakage (gray), respectively. An ordinary Raman spectrum of BDT powder (brown) is displayed for comparison. Laser excitation: 785 nm. (f) The distributions of the conductance deviations from the master curve within the high conductance (red) and low conductance (green) regimes. Bin size: 0.02. (g) The hypothesized evolution of the microscopic configuration as the conductance evolves from high conductance to low conductance.[97] (h) Schematic illustration of the simultaneous plasmonic assembly of nanoparticles and SERS. Black arrows indicate the direction of 532 nm laser (green beam) used for SPP excitation of the metal film deposited over glass cover-slip. Gray spheres are the metal nanoparticles dispersed in the water medium and red dots indicate the SERS-active molecules. Inset on the right shows the TEM image of Ag core–Au shell nanoparticle used in this experiment. Scale bar is 20 nm. (i) Schematic representation of dual assembly of Ag nanoparticles on Au film coupled to a prism: green lines are the two laser beams of 532 nm introduced at two opposite ends of the prism. Black arrows indicate the direction of the laser beams.[98] Figures reprinted with permission: (a)–(c) Ref. 96, © 2010 by the American Chemical Society; (d)–(g) Ref. 97, © 2018 by the Royal Society of Chemistry; and (h) and (i) Ref. 98, © 2014 by the Nature Publishing Group.

5 Challenges for Single-Molecule SERS

With its prosperous development in recent years, single-molecule SERS, as a powerful analytical tool to study the molecular structure and behavior at the single-molecule level, has become accessible to more and more researchers. It has enabled various unprecedented experimental observations and applications, as shown in the previous sections. However, several challenges still remain to be overcome to further boost its advancement.

First, the mechanism of single-molecule SERS is still not clearly understood. Even though EM and CM have achieved great success in explanation and interpretation of SERS experiments in the past decades,[99–101] there are still some experimental phenomena that are hardly explained using the conventional

SERS theory, such as the subnanometer spatial resolution realized by the state-of-the-art TERS, which is introduced above. When the concentration of the target molecule is decreased down to the single-molecule level, some new physics and effects, such as the Rayleigh scattering introduced above and the quantum effect, which were previously ignored or omitted may start to play critical roles. Therefore, it is essential to revisit the SERS theory and take these new physics and effects into consideration. An extended Raman theory exclusively developed for single-molecule SERS is needed to explain the phenomena observed in the single-molecule SERS and instruct the design of single-molecule SERS substrates. Correspondingly, more newly designed experiments are required to investigate these effects and verify the extended Raman theory.

Second, the data-analysis method for decoding the statistical property of single-molecule SERS has not been fully developed.[43,102] Different from conventional SERS spectra, single-molecule SERS suffers from the signal intensity fluctuation induced by molecular motion. The intrinsic fluctuation property of single-molecule SERS requires an exclusively designed method that can effectively extract the statistical features of a set of single-molecule spectra. Two attempts may be implemented to help develop the data-analysis method. On one hand, theoretical study on molecular motion near the hotspot that includes the coupling effect of electromagnetics and thermodynamics may provide some insights for us to understand the statistical behavior of the signal intensity fluctuation. This will help us develop new data-analysis methods based on the statistical behavior. On the other hand, classical statistical methods may be exclusively selected and optimized for single-molecule SERS. Based on the establishment of a more advanced data-analysis method, the real subtle behaviors of single molecules with statistical soundness can be investigated using single-molecule SERS.

Third, single-molecule SERS substrates with high reproducibility are still hardly accessible. This is mainly due to the following two reasons. First, the SERS signal of the single molecule at the hotspot is often disturbed by uncontrollable molecular motions, representing as the signal intensity fluctuation. Second, hotspots with extremely high enhancement factors for single-molecule SERS on the substrate are usually spatially sparse, which results in the low probability of detecting single molecules at the hotspots. In addition, most single-molecule SERS substrates are still based on metallic nanostructures. The large photothermal heat generation induced by the metallic nanostructures further deteriorates the chemical stability of the detected molecule as well as the environment stability of the measurement. There is still much room for the development of new SERS substrates that overcome the above drawbacks with innovative materials or surface patterns.

6 Summary

In this review, we have provided a roadmap for achieving single-molecule SERS through different enhancement strategies for diverse applications. Starting from basic concepts and mechanisms of SERS, we introduced some characteristic features related to single-molecule SERS, such as Raman enhancement factor, intensity fluctuation, and data analysis. We then reviewed recent strategies for enhancing the Raman signal intensities of single molecules, including electromagnetic enhancement, chemical enhancement, and resonance enhancement strategies and discussed the potential strategies that further promote single-molecule SERS through new perspectives. We also presented several examples of single-molecule SERS used in various fields, including catalysis, imaging, and nanoelectronics, demonstrating its powerful utility in practical applications. Finally, we specified some challenges in the future development of single-molecule SERS and proposed their corresponding solutions. In the near future, single-molecule SERS is expected to expand the family of popular analytical tools for single-molecule characterization. We believe that more discoveries in the nanoscopic world will be witnessed with advancement of single-molecule SERS as well as related theories and applications, which will lead to fundamental breakthroughs in molecular electronics, molecular imaging, chemical catalysis, and many other fields.

Acknowledgments

This work was supported by the National Natural Science Foundation of China (Nos. 11434017 and 11804254), Guangdong Innovative and Entrepreneurial Research Team Program (No. 2016ZT06C594), and National Key R&D Program of China (No. 2018YFA 0306200), Science and Technology Projects of Jiangmen [Nos. (2017)307 and 149], Program for Innovative Research Team of Jiangmen [No. (2017)385], Science and Technology Projects of Guangdong Province (No. 2016A020225009), Program for Key Basic Research of Guangdong (No. 2017KZDXM083), Cooperative Education Platform of Guangdong Province [No. (2016)31], Innovative Research Team in University of Guangdong (No. 2015KCXTD027), Key Laboratory of Optoelectronic Materials and Applications in Guangdong Higher Education (No. 2017KSYS011), and 2014 Leap Project Center of Education Department Key Platform Construction in Guangdong Province (No. GCZX-A1411).

References

1. K. A. Willets et al., "Super-resolution imaging of SERS hot spots," *Chem. Soc. Rev.* **43**(11), 3854–3864 (2014).
2. S. Laing et al., "Surface-enhanced Raman spectroscopy for *in vivo* biosensing," *Nat. Rev. Chem.* **1**(8), 0060 (2017).
3. D. K. Lim et al., "Highly uniform and reproducible surface-enhanced Raman scattering from DNA-tailorable nanoparticles with 1-nm interior gap," *Nat. Nanotechnol.* **6**(7), 452–460 (2011).
4. M. Caldarola et al., "Non-plasmonic nanoantennas for surface enhanced spectroscopies with ultra-low heat conversion," *Nat. Commun.* **6**(1), 7915 (2015).
5. E. C. Le Ru and P. G. Etchegoin, "Single-molecule surface-enhanced Raman spectroscopy," *Annu. Rev. Phys. Chem.* **63**(1), 65–87 (2012).
6. X. Shi et al., "Enhanced water splitting under modal strong coupling conditions," *Nat. Nanotechnol.* **13**(10), 953–958 (2018).
7. T. Itoh, Y. S. Yamamoto, and Y. Ozaki, "Plasmon-enhanced spectroscopy of absorption and spontaneous emissions explained using cavity quantum optics," *Chem. Soc. Rev.* **46**(13), 3904–3921 (2017).
8. S. Cong et al., "Noble metal-comparable SERS enhancement from semiconducting metal oxides by making oxygen vacancies," *Nat. Commun.* **6**(1), 7800 (2015).
9. Y. S. Yamamoto and T. Itoh, "Why and how do the shapes of surface-enhanced Raman scattering spectra change? Recent progress from mechanistic studies," *J. Raman Spectrosc.* **47**(1), 78–88 (2016).
10. S. Y. Ding et al., "Nanostructure-based plasmon-enhanced Raman spectroscopy for surface analysis of materials," *Nat. Rev. Mater.* **1**, 16021 (2016).

11. J. F. Li et al., "Shell-isolated nanoparticle-enhanced Raman spectroscopy," *Nature* **464**(7287), 392–395 (2010).
12. C. M. Aikens, L. R. Madison, and G. C. Schatz, "Raman spectroscopy: the effect of field gradient on SERS," *Nat. Photonics* **7**(7), 508–510 (2013).
13. A. G. Brolo, "Plasmonics for future biosensors," *Nat. Photonics* **6**(11), 709–713 (2012).
14. Y. He et al., "Silicon nanowires-based highly-efficient SERS-active platform for ultrasensitive DNA detection," *Nano Today* **6**(2), 122–130 (2011).
15. P. A. Dmitriev et al., "Resonant Raman scattering from silicon nanoparticles enhanced by magnetic response," *Nanoscale* **8**(18), 9721–9726 (2016).
16. D. Y. Wu et al., "Electrochemical surface-enhanced Raman spectroscopy of nanostructures," *Chem. Soc. Rev.* **37**(5), 1025–1041 (2008).
17. J. R. Lombardi et al., "A unified view of surface-enhanced Raman scattering," *Acc. Chem. Res.* **42**(6), 734–742 (2009).
18. S. M. Wells et al., "Silicon nanopillars for field-enhanced surface spectroscopy," *ACS Nano* **6**(4), 2948–2959 (2012).
19. W. H. Park et al., "Out-of-plane directional charge transfer-assisted chemical enhancement in the surface-enhanced Raman spectroscopy of a graphene monolayer," *J. Phys. Chem. C* **120**(42), 24354–24359 (2016).
20. S. M. Feng et al., "Ultrasensitive molecular sensor using n-doped graphene through enhanced Raman scattering," *Sci. Adv.* **2**(7), e1600322 (2016).
21. X. Ling et al., "Can graphene be used as a substrate for Raman enhancement?" *Nano Lett.* **10**(2), 553–561 (2010).
22. X. Ling et al., "Raman enhancement effect on two-dimensional layered materials: graphene, h-BN and MoS_2," *Nano Lett.* **14**(6), 3033–3040 (2014).
23. Z. H. Zheng et al., "Semiconductor SERS enhancement enabled by oxygen incorporation," *Nat. Commun.* **8**, 1993 (2017).
24. A. Musumeci et al., "SERS of semiconducting nanoparticles (TiO_2 hybrid composites)," *J. Am. Chem. Soc.* **131**(17), 6040–6041 (2009).
25. L. Yang et al., "A novel ultra-sensitive semiconductor SERS substrate boosted by the coupled resonance effect," *Adv. Sci.* **6**(12), 1900310 (2019).
26. H. Xu et al., "Spectroscopy of single hemoglobin molecules by surface enhanced Raman scattering," *Phys. Rev. Lett.* **83**(21), 4357–4360 (1999).
27. K. Kneipp et al., "Single molecule detection using surface-enhanced Raman scattering (SERS)," *Phys. Rev. Lett.* **78**(9), 1667–1670 (1997).
28. S. Nie et al., "Probing single molecules and single nanoparticles by surface-enhanced Raman scattering," *Science* **275**(5303), 1102–1106 (1997).
29. Z. Zhang et al., "Single molecule level plasmonic catalysis: a dilution study of *p*-nitrothiophenol on gold dimers," *Chem. Commun.* **51**(15), 3069–3072 (2015).
30. B. de Nijs et al., "Plasmonic tunnel junctions for single-molecule redox chemistry," *Nat. Commun.* **8**(1), 994–1001 (2017).
31. K. Zhang et al., "Direct SERS tracking of a chemical reaction at a single 13 nm gold nanoparticle," *Chem. Sci.* **10**(6), 1741–1745 (2019).
32. S. Jiang et al., "Distinguishing adjacent molecules on a surface using plasmon-enhanced Raman scattering," *Nat. Nanotechnol.* **10**(10), 865–869 (2015).
33. S. Jiang et al., "Subnanometer-resolved chemical imaging via multivariate analysis of tip-enhanced Raman maps," *Light Sci. Appl.* **6**(11), e17098 (2017).
34. J. Lee et al., "Microscopy with a single-molecule scanning electrometer," *Sci. Adv.* **4**(6), eaat5472 (2018).
35. Y. Li et al., "Voltage tuning of vibrational mode energies in single-molecule junctions," *Proc. Natl. Acad. Sci. U. S. A.* **111**(4), 1282–1287 (2014).
36. R. Han et al., "Investigation of charge transfer at the TiO_2–MBA–Au interface based on surface-enhanced Raman scattering: SPR contribution," *Phys. Chem. Chem. Phys.* **20**, 5666–5673 (2018).
37. C. Artur et al., "Temperature dependence of the homogeneous broadening of resonant Raman peaks measured by single-molecule surface-enhanced Raman spectroscopy," *J. Phys. Chem. Lett.* **2**(23), 3002–3005 (2011).
38. S. Yampolsky et al., "Seeing a single molecule vibrate through time-resolved coherent anti-Stokes Raman scattering," *Nat. Photonics* **8**(8), 650–656 (2014).
39. X. Chen et al., "High-resolution tip-enhanced Raman scattering probes sub-molecular density changes," *Nat. Commun.* **10**, 2567 (2019).
40. N. C. Lindquist et al., "High-speed imaging of surface-enhanced Raman scattering fluctuations from individual nanoparticles," *Nat. Nanotechnol.* **14**(10), 981–987 (2019).
41. S. Hayashi and Y. Okada, "Ultrafast superresolution fluorescence imaging with spinning disk confocal microscope optics," *Mol. Biol. Cell* **26**(9), 1743–1751 (2015).
42. A. B. Evlyukhin et al., "Demonstration of magnetic dipole resonances of dielectric nanospheres in the visible region," *Nano Lett.* **12**(7), 3749–3755 (2012).
43. P. G. Etchegoin and E. C. Le Ru, "A perspective on single molecule SERS: current status and future challenges," *Phys. Chem. Chem. Phys.* **10**(40), 6079–6089 (2008).
44. M. D. Morris and D. J. Wallan, "Resonance Raman spectroscopy. Current applications and prospects," *Anal. Chem.* **51**(2), 182A–192A (1979).
45. E. C. Le Ru et al., "Enhancement factor distribution around a single surface-enhanced Raman scattering hot spot and its relation to single molecule detection," *J. Chem. Phys.* **125**, 204701 (2006).
46. K. Kneipp et al., "Population pumping of excited vibrational states by spontaneous surface-enhanced Raman scattering," *Phys. Rev. Lett.* **76**, 2444–2447 (1996).
47. D. Wang et al., "Directional Raman scattering from single molecules in the feed gaps of optical antennas," *Nano Lett.* **13**(5), 2194–2198 (2013).
48. Y. Zhang et al., "Coherent anti-Stokes Raman scattering with single-molecule sensitivity using a plasmonic Fano resonance," *Nat. Commun.* **5**(1), 4424–4430 (2014).
49. P. C. Andersen, M. L. Jacobson, and K. L. Rowlen, "Flashy silver nanoparticles," *J. Phys. Chem. B* **108**(7), 2148–2153 (2004).
50. W. E. Doering and S. Nie, "Single-molecule and single-nanoparticle SERS: examining the roles of surface active sites and chemical enhancement," *J. Phys. Chem. B* **106**(2), 311–317 (2002).
51. J. Jiang et al., "Single molecule Raman spectroscopy at the junctions of large Ag nanocrystals," *J. Phys. Chem. B* **107**(37), 9964–9972 (2003).
52. K. A. Bosnick, J. Jiang, and L. E. Brus, "Fluctuations and local symmetry in single-molecule rhodamine 6G Raman scattering on silver nanocrystal aggregates," *J. Phys. Chem. B* **106**(33), 8096–8099 (2002).
53. K. Imura et al., "Visualization of localized intense optical fields in single gold-nanoparticle assemblies and ultrasensitive Raman active sites," *Nano Lett.* **6**(10), 2173–2176 (2006).
54. E. C. Le Ru, M. Meyer, and P. G. Etchegoin, "Proof of single-molecule sensitivity in surface enhanced Raman scattering (SERS) by means of a two-analyte technique," *J. Phys. Chem. B* **110**(4), 1944–1948 (2006).
55. E. Blackie et al., "Bi-analyte SERS with isotopically edited dyes," *Phys. Chem. Chem. Phys.* **10**(28), 4147–4153 (2008).
56. R. H. Lahr and P. J. Vikesland, "Surface-enhanced Raman spectroscopy (SERS) cellular imaging of intracellularly biosynthesized gold nanoparticles," *ACS Sustainable Chem. Eng.* **2**(7), 1599–1608 (2014).

57. J. Lin et al., "Surface-enhanced Raman scattering spectroscopy for potential noninvasive nasopharyngeal cancer detection," *J. Raman Spectrosc.* **44**(3), 497–502 (2013).
58. A. Geeraerts et al., "Systematic palynology in Ebenaceae with focus on Ebenoideae: morphological diversity and character evolution," *Rev. Palaeobot. Palynol.* **153**(3–4), 336–353 (2009).
59. E. C. Le Ru et al., "Proof of single-molecule sensitivity in surface enhanced Raman scattering (SERS) by means of a two-analyte technique," *J. Phys. Chem. B* **110**(4), 1944–1948 (2006).
60. Z. Fang et al., "Rapid classification of honey varieties by surface enhanced Raman scattering combining with deep learning," in *Cross Strait Quad-Regional Radio Sci. and Wireless Technol. Conf.* (2018).
61. Z.-Y. Li, "Mesoscopic and microscopic strategies for engineering plasmon-enhanced Raman scattering," *Adv. Opt. Mater.* **6**(16), 1701097 (2018).
62. M. Fleischmann, P. J. Hendra, and A. J. McQuillan, "Raman spectra of pyridine adsorbed at a silver electrode," *Chem. Phys. Lett.* **26**(2), 163–166 (1974).
63. D. L. Jeanmaire and R. P. Van Duyne, "Surface Raman spectroelectrochemistry: part I. Heterocyclic, aromatic, and aliphatic amines adsorbed on the anodized silver electrode," *J. Electroanal. Chem. Interfacial Electrochem.* **84**(1), 1–20 (1977).
64. M. G. Albrecht and J. A. Creighton, "Anomalously intense Raman spectra of pyridine at a silver electrode," *J. Am. Chem. Soc.* **99**(15), 5215–5217 (1977).
65. W. Li et al., "Dimers of silver nanospheres: facile synthesis and their use as hot spots for surface-enhanced Raman scattering," *Nano Lett.* **9**(1), 485–490 (2009).
66. H. Wei et al., "Polarization dependence of surface-enhanced Raman scattering in gold nanoparticle–nanowire systems," *Nano Lett.* **8**(8), 2497–2502 (2008).
67. H. Tamaru et al., "Resonant light scattering from individual Ag nanoparticles and particle pairs," *Appl. Phys. Lett.* **80**(10), 1826–1828 (2002).
68. E. J. Blackie et al., "Single-molecule surface-enhanced Raman spectroscopy of nonresonant molecules," *J. Am. Chem. Soc.* **131**(40), 14466–14472 (2009).
69. D. K. Lim et al., "Nanogap-engineerable Raman-active nanodumbbells for single-molecule detection," *Nat. Mater.* **9**(1), 60–67 (2010).
70. V. V. Thacker et al., "DNA origami based assembly of gold nanoparticle dimers for surface-enhanced Raman scattering," *Nat. Commun.* **5**(1), 3448–3454 (2014).
71. J. Fang et al., "Gold mesostructures with tailored surface topography and their self-assembly arrays for surface-enhanced Raman spectroscopy," *Nano Lett.* **10**(12), 5006–5013 (2010).
72. Z. Liu et al., "Revealing the molecular structure of single-molecule junctions in different conductance states by fishing-mode tip-enhanced Raman spectroscopy," *Nat. Commun.* **2**(1), 305 (2011).
73. R. Zhang et al., "Chemical mapping of a single molecule by plasmon-enhanced Raman scattering," *Nature* **498**(7452), 82–86 (2013).
74. J. Li et al., "Direct laser writing of symmetry-broken spiral tapers for polarization-insensitive three-dimensional plasmonic focusing," *Laser Photonics Rev.* **8**(4), 602–609 (2014).
75. J. Mu et al., "Direct laser writing of pyramidal plasmonic structures with apertures and asymmetric gratings towards efficient subwavelength light focusing," *Opt. Express* **23**(17), 22564–22571 (2015).
76. E. C. Lin et al., "Effective localized collection and identification of airborne species through electrodynamic precipitation and SERS-based detection," *Nat. Commun.* **4**(1), 1636 (2013).
77. C. Chen et al., "High spatial resolution nanoslit SERS for single-molecule nucleobase sensing," *Nat. Commun.* **9**(1), 1733 (2018).
78. P. Mao et al., "Broadband single molecule SERS detection designed by warped optical spaces," *Nat. Commun.* **9**(1), 5428 (2018).
79. S. Yang et al., "Ultrasensitive surface-enhanced Raman scattering detection in common fluids," *Proc. Natl. Acad. Sci. U. S. A.* **113**(2), 268–273 (2016).
80. J. R. Lombardi et al., "Charge- transfer theory of surface enhanced Raman spectroscopy: Herzberg–Teller contributions," *J. Chem. Phys.* **84**(8), 4174–4180 (1986).
81. P. Hildebrandt and M. Stockburger, "Surface-enhanced resonance Raman spectroscopy of rhodamine 6G adsorbed on colloidal silver," *J. Phys. Chem.* **88**(24), 5935–5944 (1984).
82. P. Hildebrand and M. Stockburger, "Surface-enhanced resonance Raman spectroscopy of cytochrome c at room and low temperatures," *J. Phys. Chem.* **90**(22), 6017–6024 (1986).
83. E. K. Pozzi et al., "Ultrahigh-vacuum tip-enhanced Raman spectroscopy," *Chem. Rev.* **117**(7), 4961–4982 (2017).
84. Z. L. Zhang et al., "Tip-enhanced Raman spectroscopy," *Anal. Chem.* **88**(19), 9328–9346 (2016).
85. A. B. Zrimsek et al., "Single-molecule chemistry with surface- and tip-enhanced Raman spectroscopy," *Chem. Rev.* **117**(11), 7583–7613 (2017).
86. X. Shi et al., "Advances in tip-enhanced near-field Raman microscopy using nanoantennas," *Chem. Rev.* **117**(7), 4945–4960 (2017).
87. P. Verma, "Tip-enhanced Raman spectroscopy: technique and recent advances," *Chem. Rev.* **117**(9), 6447–6466 (2017).
88. M. Richard-Lacroix et al., "Mastering high resolution tip-enhanced Raman spectroscopy: towards a shift of perception," *Chem. Soc. Rev.* **46**(13), 3922–3944 (2017).
89. X. Wang et al., "Tip-enhanced Raman spectroscopy for surfaces and interfaces," *Chem. Soc. Rev.* **46**(13), 4020–4041 (2017).
90. C. Zhang, B. Q. Chen, and Z. Y. Li, "Optical origin of subnanometer resolution in tip-enhanced Raman mapping," *J. Phys. Chem. C* **119**(21), 11858–11871 (2015).
91. M. J. Limo et al., "Interactions between metal oxides and biomolecules: from fundamental understanding to applications," *Chem. Rev.* **118**(22), 11118–11193 (2018).
92. A. B. Djurisic et al., "Toxicity of metal oxide nanoparticles: mechanisms, characterization, and avoiding experimental artefacts," *Small* **11**(1), 26–44 (2015).
93. L. Da Via et al., "Visible light selective photocatalytic conversion of glucose by TiO_2," *Appl. Catal. B* **202**, 281–288 (2017).
94. N. Chen et al., "Electronic logic gates from three-segment nanowires featuring two p-n heterojunctions," *NPG Asia Mater.* **5**(8), e59–e63 (2013).
95. K. E. Shafer-Peltier et al., "Toward a glucose biosensor based on surface-enhanced Raman scattering," *J. Am. Chem. Soc.* **125**(2), 588–593 (2003).
96. E. Cortes et al., "Monitoring the electrochemistry of single molecules by surface-enhanced Raman spectroscopy," *J. Am. Chem. Soc.* **132**(51), 18034–18037 (2010).
97. J. Zheng et al., "Electrical and SERS detection of disulfide-mediated dimerization in single-molecule benzene-1,4-dithiol junctions," *Chem. Sci.* **9**, 5033–5038 (2018).
98. P. P. Patra et al., "Plasmofluidic single-molecule surface-enhanced Raman scattering from dynamic assembly of plasmonic nanoparticles," *Nat. Commun.* **5**, 4357 (2014).
99. K. L. Kelly et al., "The optical properties of metal nanoparticles: the influence of size, shape, and dielectric environment," *J. Phys. Chem. B* **107**(3), 668–677 (2003).
100. A. Otto, "What is observed in single molecule SERS, and why?" *J. Raman Spectrosc.* **33**(8), 593–598 (2002).
101. D. P. Tsai et al., "Photon scanning tunneling microscopy images of optical excitations of fractal metal colloid clusters," *Phys. Rev. Lett.* **72**(26), 4149–4152 (1994).
102. P. G. Etchegoin et al., "Statistics of single-molecule surface enhanced Raman scattering signals: fluctuation analysis with multiple analyte techniques," *Anal. Chem.* **79**(21), 8411–8415 (2007).

Yang Yu received his BS degree in physics and electronic science from Shandong Normal University, Jinan, in 2009, and his PhD in optics from the Institute of Physics, Chinese Academy of Sciences, Beijing, in 2017. He is now a lecturer of the School of Applied Physics and Materials at Wuyi University, Jiangmen. His research interests cover the theory and experiment of micro/nanofiber-based devices and sensors.

Ting-Hui Xiao received his BS degree in optical information science and technology from Sun Yat-sen University in 2013, his MS degree in optics from the Institute of Physics, Chinese Academy of Sciences in 2016, and his PhD in chemistry from University of Tokyo in 2019. Now, he is an assistant professor at the Department of Chemistry, University of Tokyo. His research interests cover the theory and experiment of silicon photonics, nanophotonics, vibrational spectroscopy, and ultrafast optics.

Zhi-Yuan Li received his BS degree in optoelectronics from the University of Science and Technology of China, Hefei, in 1994, and his PhD in optics from the Institute of Physics, Chinese Academy of Sciences, Beijing, in 1999, where he served as a principal investigator during 2004–2016. He is now a professor and associate dean of the School of Physics and Optoelectronics at the South China University of Technology, Guangzhou. His research interests cover the theory and experiment of photonic crystals, metamaterials, plasmonics, nonlinear and ultrafast optics, laser technology, quantum optics, quantum physics, and optical tweezers.

Biographies of the other authors are not available.